

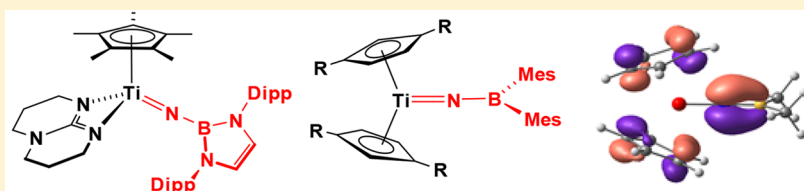
New Titanium Borylimido Compounds: Synthesis, Structure, and Bonding

Benjamin A. Clough,[†] Simona Mellino,[†] Andrey V. Protchenko,[†] Martin Slusarczyk,[†] Laura C. Stevenson,[†] Matthew P. Blake,[†] Bowen Xie,[†] Eric Clot,^{*,‡} and Philip Mountford^{*,†}

[†]Chemistry Research Laboratory, Department of Chemistry, University of Oxford, Mansfield Road, Oxford OX1 3TA, U.K.

[‡]Institut Charles Gerhardt Montpellier, UMR 5253, CNRS-UM-ENSCM, Université de Montpellier, cc 1501, Place Eugène Bataillon, F-34095 Montpellier Cedex 5, France

S Supporting Information



ABSTRACT: We report a combined experimental and computational study of the synthesis and electronic structure of titanium borylimido compounds. Three new synthetic routes to this hitherto almost unknown class of Group 4 imide are presented. The double-deprotonation reaction of the borylamine $\text{H}_2\text{NB}(\text{NAr}'\text{CH})_2$ ($\text{Ar}' = 2,6\text{-C}_6\text{H}_3\text{Pr}_2$) with $\text{Ti}(\text{NMe}_2)_2\text{Cl}_2$ gave $\text{Ti}\{\text{NB}(\text{NAr}'\text{CH})_2\}\text{Cl}_2(\text{NHMe}_2)_2$, which was easily converted to $\text{Ti}\{\text{NB}(\text{NAr}'\text{CH})_2\}\text{Cl}_2(\text{py})_3$. This compound is an entry point to other borylimides, for example, reacting with $\text{Li}_2\text{N}_2^{\text{pyr}}\text{N}^{\text{Me}}$ to form $\text{Ti}(\text{N}_2^{\text{pyr}}\text{N}^{\text{Me}})\{\text{NB}(\text{NAr}'\text{CH})_2\}(\text{py})_2$ and with 2 equiv of NaCp to give $\text{Cp}_2\text{Ti}\{\text{NB}(\text{NAr}'\text{CH})_2\}(\text{py})$ (**23**). Borylamine-*tert*-butylimide exchange between $\text{H}_2\text{NB}(\text{NAr}'\text{CH})_2$ and $\text{Cp}^*\text{Ti}(\text{N}^t\text{Bu})\text{Cl}(\text{py})$ under forcing conditions afforded $\text{Cp}^*\text{Ti}\{\text{NB}(\text{NAr}'\text{CH})_2\}\text{Cl}(\text{py})$, which could be further substituted with guanidinate or pyrrolide-amine ligands to give $\text{Cp}^*\text{Ti}(\text{hpp})\{\text{NB}(\text{NAr}'\text{CH})_2\}$ (**16**) and $\text{Cp}^*\text{Ti}(\text{N}^{\text{pyr}}\text{N}^{\text{Me}}_2)\{\text{NB}(\text{NAr}'\text{CH})_2\}$ (**17**). The $\text{Ti}-\text{N}_{\text{im}}$ distances in compounds with the $\text{NB}(\text{NAr}'\text{CH})_2$ ligand were comparable to those of the corresponding arylimides. Dialkyl- or diaryl-substituted borylamines do not undergo the analogous double-deprotonation or imide-amine exchange reactions. Reaction of $(\text{Cp}''_2\text{Ti})_2(\mu_2:\eta^1, \eta^1\text{-N}_2)$ with N_3BMes_2 gave the base-free, diarylborylimide $\text{Cp}''_2\text{Ti}(\text{NBMe}_2)_2$ (**26**) by an oxidative route; this compound has a relatively long $\text{Ti}-\text{N}_{\text{im}}$ bond and large $\text{Cp}''-\text{Ti}-\text{Cp}''$ angle. Reaction of **16** with $\text{H}_2\text{N}^t\text{Bu}$ formed equilibrium mixtures with $\text{H}_2\text{NB}(\text{NAr}'\text{CH})_2$ and $\text{Cp}^*\text{Ti}(\text{hpp})(\text{N}^t\text{Bu})$ ($\Delta_r G = -1.0 \text{ kcal mol}^{-1}$). In contrast, the dialkylborylimide $\text{Cp}^*\text{Ti}\{\text{MeC}(\text{N}^t\text{Pr})_2\}(\text{NBC}_8\text{H}_{14})$ (**2**) reacted quantitatively with $\text{H}_2\text{N}^t\text{Bu}$ to give the corresponding *tert*-butylimide and borylamine. The electronic structures and imide-amine exchange reactions of half-sandwich and sandwich titanium borylimides have been evaluated using density functional theory (DFT), supported by quantum theory of atoms in molecules (QTAIM) and natural bond orbital (NBO) analysis, and placed more generally in context with the well-established alkyl- and arylimides and hydrazides. The calculations find that $\text{Ti}-\text{N}_{\text{im}}$ bonds for borylimides are stronger and more covalent than in their organoimido or hydrazido analogues, and are strongest for alkyl- and arylborylimides. Borylamine-*tert*-butylimide exchange reactions fail for H_2NBR_2 ($\text{R} = \text{hydrocarbyl}$) but not for $\text{H}_2\text{NB}(\text{NAr}'\text{CH})_2$ because the increased strength of the new $\text{Ti}-\text{N}_{\text{im}}$ bond for the former is outweighed by the increased net $\text{H}-\text{N}$ bond strengths in the borylamine. Variation of the $\text{Ti}-\text{N}_{\text{im}}$ bond length over short distances is dominated by π -interactions with any appropriate orbital on the N_{im} atom organic substituent. However, over the full range of imides and hydrazides studied, overall bond energies do not correlate with bond length but with the $\text{Ti}-\text{N}_{\text{im}}$ σ -bond character and the orthogonal π -interaction.

INTRODUCTION

As summarized in several reviews,¹ the synthesis, bonding, and reactivity of Group 4 terminal organoimido complexes $(\text{L})\text{M}(\text{NR})$ ($\text{M} = \text{Group 4 metal}$, $\text{R} = \text{alkyl or aryl}$) have seen considerable activity since Bergman, Wolczanski, Rothwell, and Roesky's initial reports in these areas.² The polar and unsaturated $\text{M}-\text{N}_{\text{im}}$ multiple bond (formally a $\sigma^2\pi^4$ triple bond in most instances³) usually acts as the reactive site in these complexes and can undergo a wide range of addition reactions with saturated and unsaturated substrates. In addition to the continuing interest in Group 4 imido chemistry, the past 10

years in particular have seen a number of advances in the corresponding dialkyl- or diarylhydrazido(2-) complexes $(\text{L})\text{M}(\text{NNR}_2)$ ($\text{M} = \text{Group 4}$, $\text{R} = \text{alkyl or aryl}$)⁴ where the hydrocarbyl N_{im} -substituent of an organoimido group is replaced by a heteroatom donor. This chemistry, following from initial reports by Wiberg⁵ and Bergman,^{4b} is also characterized by single or multiple coupling or insertion reactions of the $\text{M}-\text{N}_{\text{im}}$ bond. On reaction with reducing

Received: July 19, 2017

Published: August 24, 2017

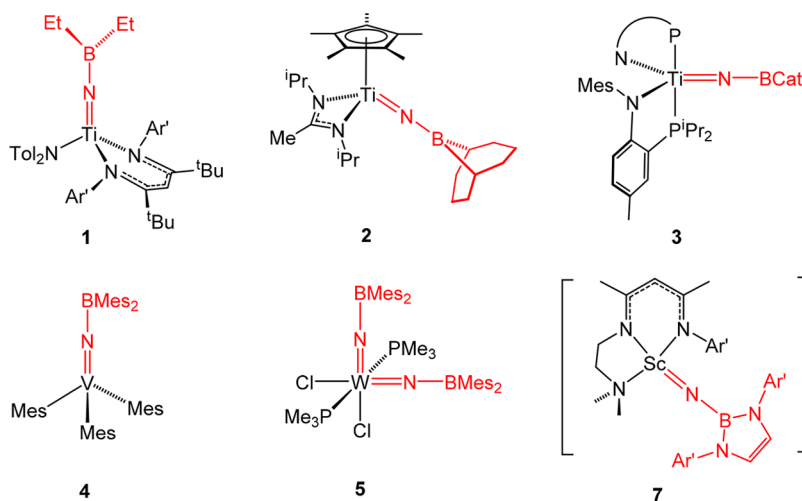


Figure 1. Isolated and transient terminal borylimido complexes of Groups 3–6. Ar' = 2,6-C₆H₃iPr₂, Mes = 2,4,6-C₆H₂Me₃, N⋯P = MesN-1,2-C₆H₄PiPr₂, BCat = B(1,2-O₂C₆H₄).^{4q,10–13,15}

substrates such as alkynes, CO, and isonitriles, cleavage of the N_{im}–NR₂ bond can also occur. In further development of heteroatom-functionalized imido compounds we showed that the corresponding alkoxyimido, (L)Ti(NOR), chemistry can also be readily accessed, leading in certain cases to reductive N_{im}–O bond cleavage and/or Ti–N_{im} addition and coupling reactions.⁶

The N_{im}-bound heteroatom donors in hydrazido and alkoxyimido compounds perturb the bonding in the Ti–N_{im} bond itself by acting as lone pair (π) donors to one of the Ti–N_{im} π* MOs (MO = molecular orbital), and also destabilizing one of the Ti–N_{im} π-bond MOs. We have reported density functional theory (DFT) and natural bond orbital (NBO)⁷ studies of these effects, including the cyclopentadienylamidinate complexes Cp*Ti{MeC(NⁱPr)₂}(NR) (R = hydrocarbyl, NR'₂ or OR'), which can be prepared for a range of imido and related functional groups.^{3h,4r,6b,8}

In contrast to this well-developed literature for Group 4 organoimido, hydrazido, and alkoxyimido chemistry, very little indeed is known about borylimido compounds (L)Ti(NBR₂) (R = hydrocarbyl or heteroatom donor moiety). These feature a strongly σ-donating⁹ but π-accepting BR₂ substituent at N_{im}. The first Group 4 borylimide was Mindiola's **1** (Figure 1) formed unexpectedly from the corresponding parent imide (i.e., terminal NH) with 2 equiv of NaHBEt₃.¹⁰ We subsequently reported the formation of a second titanium borylimide, namely, Cp*Ti{MeC(NⁱPr)₂}(NBC₈H₁₄) (**2**, Figure 1)^{4q} through the serendipitous reductive N_{im}–NR₂ bond cleavage reaction of the hydrazides Cp*Ti{MeC(NⁱPr)₂}(NNR₂) (R = Me or Ph) with 9-BBN. Very recently a catechol-functionalized borylimide **3** was obtained by reaction of a rare metalated nitride with ClBCat.¹¹ There are only very few other transition metal borylimides known. Wilkinson and Sundermeyer have reported the synthesis of Group 5 and 6 dimesitylborylimides (e.g., **4** and **5** in Figure 1) by the oxidative reaction of lower oxidation state precursors with N₃BMe₂,¹² and Fryzuk et al. prepared a ditantalum borylimide by reaction of 9-BBN with a dinitrogen compound.¹³ Our group very recently extended borylimido chemistry to Group 3 by using the bulky borylamine H₂NB(NAr'CH)₂ (**6**)¹⁴ to access the methylborylamide (NaCnac^{NMe₂})Sc(Me){NHB(NAr'CH)₂}.¹⁵ Thermolysis led to methane elimination and formation of the

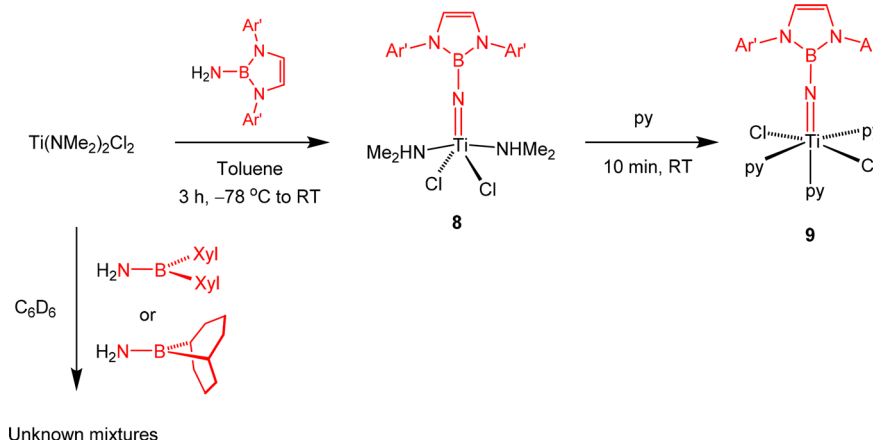
transient borylimide **7** (Figure 1, neither isolated nor observed) which was trapped by [2 + 2] cycloaddition or C–H bond activation reactions. These are the first substrate-activation reactions of any metal-bound borylimide, although a number of interesting reports have appeared in the past decade concerning the small molecule activation reactions of transient borylnitrenes (generated from azide precursors).¹⁶

Encouraged by these recent results we set out to develop new routes to titanium borylimido compounds using H₂NB(NAr'CH)₂ as a representative heteroatom-substituted borylamine, and H₂NBC₈H₁₄ and H₂NBMe₂ as organoborylamine analogues. In addition to extending the range of known titanium borylimides and developing useful synthetic routes for the future, we aimed to gain a better understanding of the bonding in these types of compound, both *per se* and in the wider context of the much better-established organoimido and hydrazido analogues.

RESULTS AND DISCUSSION

Synthesis of Bis(amine) and Tris(pyridine) Titanium Borylimido Compounds. One aim of this work was to establish the scope and potential of general synthetic entry points to titanium borylimido chemistry to complement those we have demonstrated previously for their organoimido,^{1c,e,17} hydrazido,^{3h,4l,8a,18} and alkoxyimido^{6a,b,d} analogues. Bis-(dimethylamine) and tris(pyridine) compounds of the type Ti(NR)Cl₂(NHMe₂)₂ and Ti(NR)Cl₂(py)₃ (R = alkyl, aryl, NR'₂ (R' = Me and/or Ph) or O^tBu) have been particularly useful since substitution of one or more of the chloride and/or amine/pyridine ligands by other ligand sets is generally straightforward. The tris(pyridine) compounds can usually be accessed from their bis(dimethylamine) homologues. These, in turn, can be straightforwardly prepared by reaction of Ti(NMe₂)₂Cl₂ with the respective primary amine, aniline, hydrazine, or *tert*-butoxyamine. We sought to extend these routes to borylamines H₂NBR₂ where R is either an N-donor or C-donor substituent.

The N,N-disubstituted borylamine H₂NB(NAr'CH)₂ (**6**) is readily available in multigram quantities,¹⁴ and was very successfully employed in accessing scandium borylimido chemistry.¹⁵ Reaction of **6** with Ti(NMe₂)₂Cl₂ on the NMR tube scale in C₆D₆, quantitatively formed the borylimido

Scheme 1. Synthesis of $\text{Ti}\{\text{NB}(\text{NAr}'\text{CH})_2\}\text{Cl}_2(\text{NHMe}_2)_2$ (**8**) and $\text{Ti}\{\text{NB}(\text{NAr}'\text{CH})_2\}\text{Cl}_2(\text{py})_3$ (**9**)

complex $\text{Ti}\{\text{NB}(\text{NAr}'\text{CH})_2\}\text{Cl}_2(\text{NHMe}_2)_2$ (**8**) via double proton transfer (Scheme 1) from **6** to the NMe_2 ligands. On the preparative scale in toluene, **8** was isolated in 79% yield. The ^1H NMR spectrum displays resonances for a C_s symmetric species containing one $\text{NB}(\text{NAr}'\text{CH})_2$ and two NHMe_2 ligands. The ^{11}B chemical shift of the borylimido ligand in **8** is 14.2 ppm, upfield from the value of 23.0 ppm for $\text{H}_2\text{NB}(\text{NAr}'\text{CH})_2$ (**6**). DFT calculations on the full complex **8** gave a computed ^{11}B NMR shift of 13.7 ppm, which is in good agreement with the experimental value.

Diffraction-quality crystals of **8** were grown from hexane. The solid state structure is shown in Figure 2, along with selected bond lengths and angles. Compound **8** has an approximately trigonal bipyramidal geometry ($\tau = 0.19$) in which the two NHMe_2 ligands occupy the axial sites and the Cl and $\text{NB}(\text{NAr}'\text{CH})_2$ ligands occupy equatorial ones. Compound **8** can be compared with a wide range of previously structurally

characterized complexes $\text{Ti}(\text{NR})\text{Cl}_2(\text{NHMe}_2)_2$ ($\text{R} = \text{alkyl, aryl, O}^t\text{Bu}$),^{1,2,5–9} which have similar geometries. Of particular interest here is the $\text{Ti}\{\text{NB}(\text{NAr}'\text{CH})_2\}$ moiety. The short $\text{Ti}(1)–\text{N}(1)$ distance of 1.7027(10) Å and the near-linear $\text{Ti}(1)–\text{N}(1)–\text{B}(1)$ angle of 178.19(9)°, which implies sp hybridization at $\text{N}(1)$, are both indicative of a $\text{Ti}\equiv\text{N}_{\text{im}}$ triple bond ($\sigma^2\pi^4$ configuration).

Previous structural¹⁹ and computational studies have found that $\text{Ti}–\text{N}_{\text{im}}$ bond lengths typically follow the trend $\text{Ti}–\text{NR}$ ($\text{R} = \text{alkyl}$) < $\text{Ti}–\text{NO}^t\text{Bu}$ < $\text{Ti}–\text{NAr}$ < $\text{Ti}–\text{NNR}'_2$ ($\text{R}' = \text{Me}$ or Ph). The $\text{Ti}(1)–\text{N}(1)$ bond length of 1.7027(10) Å in **8** places this value within the range reported for a series of eight arylimido complexes $\text{Ti}(\text{NAr})\text{Cl}_2(\text{NHMe}_2)_2$ (av. $\text{Ti}–\text{N}_{\text{im}} = 1.703$ Å, range 1.694(4)–1.708(2) Å),^{17c,20} whereas it is longer than in both the alkylimido $\text{Ti}(\text{N}^i\text{Pr})\text{Cl}_2(\text{NHMe}_2)_2$ (1.672(2) Å) and the *tert*-butoxyimido analogue (av. 1.689(4) Å).^{6b,17c} The $\text{N}(1)–\text{B}(1)$ distance of 1.4374(16) Å is typical¹⁹ of compounds of the type $\text{R}_2\text{N}–\text{BR}'_2$ which have significant $\text{N}=\text{B}$ double bond character via $\text{N}_{2p} \rightarrow \text{B}_{2p}$ π -donation. More specifically, it is longer than in $\text{Cp}^*\text{Ti}\{\text{MeC}(\text{N}^i\text{Pr})_2\}–(\text{NBC}_6\text{H}_{14})$ (**2**, 1.402(4) Å)^{4q} but comparable to Mindiola's $\text{Ti}(\text{NBET}_2)(\text{NTol}_2)\{\text{HC}(\text{C}^t\text{BuNAr}')_2\}$ (**1**, 1.428(6) Å).¹⁰ However, the differing ligand types and coordination numbers in these three compounds renders precise comparisons of $\text{Ti}–\text{N}_{\text{im}}$ and $\text{N}_{\text{im}}–\text{B}$ distances inappropriate.

In the solid state, **8** forms hydrogen-bonded dimers (see Figure S1 of the Supporting Information). Only $\text{Cl}(2)$ and $\text{N}(4)\text{HMe}_2$ are involved in an $\text{N}–\text{H}\cdots\text{Cl}$ hydrogen bond, the $\text{H}(1)\cdots\text{Cl}(2\text{A})$ distance of 2.86(2) Å lying within the expected range for an “intermediate” strength $\text{N}–\text{H}\cdots\text{Cl}$ hydrogen bond.²² This causes the longer $\text{Ti}(1)–\text{Cl}(2)$ distance of 2.3730(4) Å compared to $\text{Ti}(1)–\text{Cl}(1)$ (2.3224(4) Å). The solid state IR spectrum (Nujol mull) of **8** is consistent with this, showing two $\nu(\text{N}–\text{H})$ bands at 3289 and 3277 cm^{-1} , assigned to the nonbridging $\text{N}–\text{H}$ bond and the hydrogen bonding $\text{N}–\text{H}$, respectively. In dichloromethane solution, a single $\nu(\text{N}–\text{H})$ band is observed at 3288 cm^{-1} . Hydrogen-bonded motifs (chains or dimers) have been reported for many compounds of the type $\text{Ti}(\text{NR})\text{Cl}_2(\text{NHMe}_2)_2$.^{17c,20}

Reactions were also carried out between $\text{Ti}(\text{NMe}_2)_2\text{Cl}_2$ and $\text{H}_2\text{NBC}_8\text{H}_{14}$ or H_2NBMe_2 (Scheme 1) in an attempt to make the corresponding diorganoborylimido complexes. The reaction of H_2NBMe_2 with $\text{Ti}(\text{NMe}_2)_2\text{Cl}_2$ on the NMR tube scale in C_6D_6 at 50 °C (no reaction occurred at room temperature) formed a complex mixture of unknown products. Reaction with

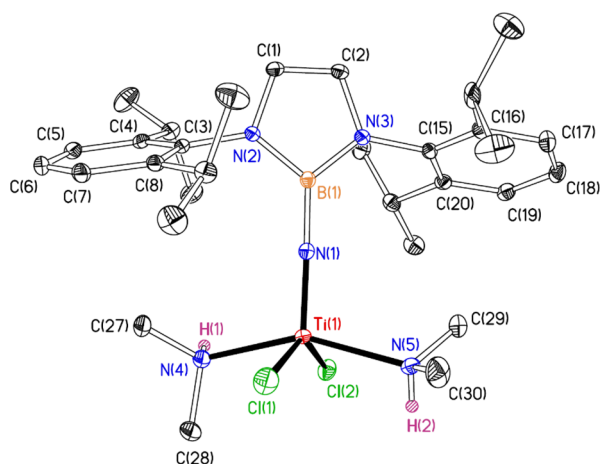


Figure 2. Displacement ellipsoid plot (25% probability) of $\text{Ti}\{\text{NB}(\text{NAr}'\text{CH})_2\}\text{Cl}_2(\text{NHMe}_2)_2$ (**8**). C-bound H atoms are omitted for clarity. H(1) and H(2) are drawn as spheres of an arbitrary radius. Selected bond distances (Å) and angles (°): $\text{Ti}(1)–\text{N}(1)$ 1.7027(10), $\text{Ti}(1)–\text{N}(4)$ 2.2235(11), $\text{Ti}(1)–\text{N}(5)$ 2.2447(11), $\text{Ti}(1)–\text{Cl}(1)$ 2.3224(4), $\text{Ti}(1)–\text{Cl}(2)$ 2.3730(4), $\text{N}(1)–\text{B}(1)$ 1.4374(16), $\text{N}(4)–\text{H}(1)$ 0.898(18), $\text{N}(5)–\text{H}(2)$ 0.849(19), $\text{N}(1)–\text{Ti}(1)–\text{N}(4)$ 104.60(4), $\text{N}(1)–\text{Ti}(1)–\text{N}(5)$ 102.30(4), $\text{N}(4)–\text{Ti}(1)–\text{N}(5)$ 152.65(4), $\text{N}(1)–\text{Ti}(1)–\text{Cl}(1)$ 110.35(4), $\text{N}(1)–\text{Ti}(1)–\text{Cl}(2)$ 108.21(4), $\text{Cl}(1)–\text{Ti}(1)–\text{Cl}(2)$ 141.288(17), $\text{Ti}(1)–\text{N}(1)–\text{B}(1)$ 178.19(9); $\tau = 0.19$.²¹

$\text{H}_2\text{NBC}_8\text{H}_{14}$ also resulted in unknown products except for the known aminoborane²³ $\text{Me}_2\text{NBC}_8\text{H}_{14}$ which could be identified from its ^1H and ^{11}B NMR data. $\text{Me}_2\text{NBC}_8\text{H}_{14}$ is possibly formed by an unproductive transamination reaction between a Ti-bound NMe_2 ligand and the NH_2 group of the borylamine, but the complex nature of the reaction product mixture precludes further speculation.

Given how little is known of these types of transamination reactions of borylamines with metal complexes, and the previously versatile nature of the amine-to-imide reactions of $\text{Ti}(\text{NMe}_2)_2\text{Cl}_2$ with H_2NR , we examined selected model and full experimental systems by DFT at the B3PW91 level (see the Supporting Information for further details). The SCF energies for the model reactions of $\text{Ti}(\text{NMe}_2)_2\text{Cl}_2$ with H_2NPh , H_2NMe , $\text{H}_2\text{NB}(\text{NMeCH})_2$, H_2NBPh_2 , and H_2NBMe_2 to form the corresponding imides $\text{Ti}(\text{NR})\text{Cl}_2(\text{NHMe}_2)_2$ were -15.2 , -14.0 , -14.9 , -5.1 , and -2.5 kcal mol $^{-1}$, respectively. This shows a much reduced tendency on electronic grounds for this transformation in the case of the diorganoborylamines. Corresponding calculations (including corrections for dispersion and solvent effects (see the Supporting Information)) were also carried out on selected full experimental systems. The DFT reactions of $\text{Ti}(\text{NMe}_2)_2\text{Cl}_2$ with H_2NPh , $\text{H}_2\text{N}^t\text{Bu}$, $\text{H}_2\text{NB}(\text{NAr}'\text{CH})_2$ (**6**), H_2NBMe_2 , and monomeric $\text{H}_2\text{NBC}_8\text{H}_{14}$ gave $\Delta_r G = -9.9$, -7.8 , -4.3 , -2.0 , and $+2.3$ kcal mol $^{-1}$ at 298 K. These values confirm the underlying electronic trends, attenuated by the increased steric effects of the real substituents. The DFT results are consistent with the experimental outcomes^{17c} in the cases of H_2NPh , $\text{H}_2\text{N}^t\text{Bu}$, and **6**. In the case of H_2NBMe_2 the desired product is predicted to be thermodynamically viable, but the experimental observations show that alternative unknown and deleterious pathways are available (perhaps involving amine/amide group exchange as found with $\text{H}_2\text{NBC}_8\text{H}_{14}$). In the case of $\text{H}_2\text{NBC}_8\text{H}_{14}$ the target reaction is fairly endergonic, leading to alternative unknown pathways. We return to a detailed analysis of the factors controlling these types of exchange reaction later on.

Reaction of **8** with neat pyridine gave clean formation of $\text{Ti}\{\text{NB}(\text{NAr}'\text{CH})_2\}\text{Cl}_2(\text{py})_3$ (**9**) in 89% isolated yield (Scheme 1). We were also able to prepare compound **9** via a one-pot reaction from $\text{Ti}(\text{NMe}_2)_2\text{Cl}_2$ without the need to purify the intermediate **8**, yielding 5.3 g of **9** from 1.5 g of $\text{Ti}(\text{NMe}_2)_2\text{Cl}_2$ and 3.0 g of borylamine **6** (94% overall yield). The ^1H NMR spectrum of **9** features the expected resonances for the borylimido ligand, as well as two sets of resonances in a 2:1 integration ratio for pyridine ligands *cis* and *trans* to the borylimido group. The signals for the *trans*-pyridine are significantly broadened, an effect which has also been described in the organoimido, hydrazido, and alkoxyimido complexes,^{6b,17a,18a} and is attributed to a dissociative exchange of the more labile *trans*-pyridine ligands in solution. The ^{11}B NMR shift of 13.8 ppm is comparable to that of 14.2 ppm in **8**.

Diffraction-quality crystals of **9** were grown from hexane at 5 °C. The solid state structure is shown in Figure 3, along with selected bond lengths and angles. Compound **9** has an approximately octahedrally coordinated titanium, analogous to previous complexes of the type $\text{Ti}(\text{NR})\text{Cl}_2(\text{py})_3$ ($\text{R} = \text{alkyl}$, aryl , NPh_2 , O^tBu).^{2c,6b,8a,17a,20,24} $\text{Ti}(1)$ lies ca. 0.27 Å above the $\{\text{Cl}(1), \text{Cl}(2), \text{N}(5), \text{N}(6)\}$ least-squares plane in order to enhance the $\text{Ti}(1)-\text{N}(1)$ π -bonding, as described for certain imido and nitrido complexes.^{3d,25} The $\text{Ti}(1)-\text{N}(1)$ bond length of 1.7118(9) Å is again indicative of a $\text{Ti}\equiv\text{N}_{\text{im}}$ triple bond and falls within the range of $\text{Ti}-\text{N}_{\text{im}}$ distances for

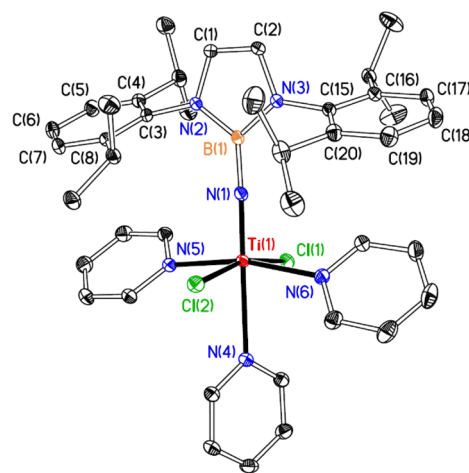
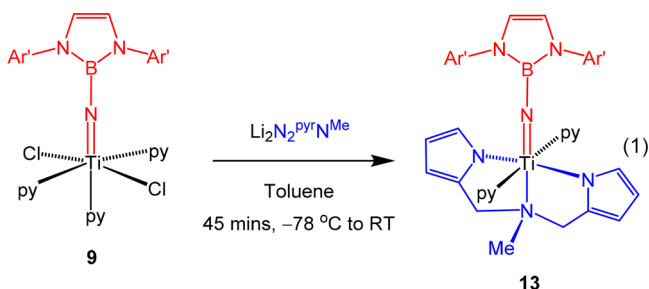


Figure 3. Displacement ellipsoid plot (30% probability) of $\text{Ti}\{\text{NB}(\text{NAr}'\text{CH})_2\}\text{Cl}_2(\text{py})_3$ (**9**). H atoms are omitted for clarity. Selected bond distances (Å) and angles (°): $\text{Ti}(1)-\text{N}(1)$ 1.7118(9), $\text{Ti}-\text{N}(4)$ 2.5411(9), $\text{Ti}(1)-\text{N}(5)$ 2.2229(9), $\text{Ti}(1)-\text{N}(6)$ 2.2268(9), $\text{Ti}(1)-\text{Cl}(1)$ 2.4106(3), $\text{Ti}(1)-\text{Cl}(2)$ 2.3861(3), $\text{N}(1)-\text{B}(1)$ 1.4216(14), $\text{N}(1)-\text{Ti}(1)-\text{N}(4)$ 179.37(3), $\text{N}(1)-\text{Ti}(1)-\text{N}(5)$ 94.77(4), $\text{N}(1)-\text{Ti}(1)-\text{N}(6)$ 98.41(4), $\text{N}(1)-\text{Ti}(1)-\text{Cl}(1)$ 96.30(3), $\text{N}(1)-\text{Ti}(1)-\text{Cl}(2)$ 97.34(3), $\text{Cl}(1)-\text{Ti}(1)-\text{Cl}(2)$ 166.343(12), $\text{Ti}(1)-\text{N}(1)-\text{B}(1)$ 177.85(9).

structurally characterized arylimides $\text{Ti}(\text{NAr})\text{Cl}_2(\text{py})_3$ (av. $\text{Ti}-\text{N}_{\text{im}} = 1.718$ Å, range 1.705(4)–1.730(2) Å for six examples).^{17a,20,24a,26} $\text{Ti}(1)-\text{N}(1)$ is longer than in both the alkylimide $\text{Ti}(\text{N}^t\text{Bu})\text{Cl}_2(\text{py})_3$ (**10**, av. 1.701(4) Å)^{17a,24b} and in the alkoxyimide $\text{Ti}(\text{NO}^t\text{Bu})\text{Cl}_2(\text{py})_3$ (**11**, 1.7087(18) Å),² and shorter than in the hydrazide $\text{Ti}(\text{NNPh}_2)\text{Cl}_2(\text{py})_3$ (**12**, 1.727(2) Å).³ The $\text{N}(1)-\text{B}(1)$ bond length of 1.4216(14) Å is comparable to that in **8**.

The borylimido ligand exerts a strong *trans* influence (defined quantitatively as the difference between the $\text{Ti}-\text{N}$ bond lengths for the pyridine ligands *cis* and *trans* to the borylimido ligand) on the $\text{N}(4)$ pyridine ligand. The average lengthening of 0.316(1) Å is significantly larger than for the homologous $\text{Ti}(\text{NR})\text{Cl}_2(\text{py})_3$ ($\text{R} = ^t\text{Bu}$ (**10**), Ph , ToI , $\text{P}(\text{S})\text{Ph}_2$; range = 0.18–0.21 Å),^{2c,17a} hydrazides $\text{Ti}(\text{NNPh}_2)\text{Cl}_2(\text{L})_3$ ($\text{L} = \text{py}$ (**12**), $4\text{-NC}_5\text{H}_4^t\text{Bu}$; av. ca. 0.16 Å)³ and alkoxyimide **11** (0.170(2) Å).^{6b} The *trans* influence in such complexes depends on a number of factors, including the N_{im} -substituent and the $\text{Ti}-\text{N}_{\text{im}}$ bond distance.^{3d,17a} The large *trans* influence in the case of **9** may imply that the borylimido ligand has a very high σ -donor ability compared to its imido, hydrazido, and alkoxyimido analogues. This would be consistent with the well-developed chemistry of the $\text{B}(\text{NAr}'\text{CH})_2$ moiety, which is itself a very strong σ -donor.⁹ Calculations for the $[\text{NB}(\text{NAr}'\text{CH})_2]^{2-}$ dianion¹⁵ are consistent with this, and further DFT studies are described later in this contribution.

The borylimide **9** was specifically targeted because of its potential ability to act as a synthon for the installation of different supporting ligand sets.^{6a,b,8a,17a} As a proof of principle, the dipyrrolide-amine ligand $\text{N}_2^{\text{pyr}}\text{N}^{\text{Me}}$ (the dianion of N,N -di(pyrrolyl- α -methyl)- N -methylamine) was introduced via salt elimination. This ligand has previously been utilized by Odom in a number of imido and amido compounds relevant to small molecule activation and catalysis.^{4d,f,6b,27} Mixing **9** and $\text{Li}_2\text{N}_2^{\text{pyr}}\text{N}^{\text{Me}}$ in toluene at -78 °C, followed by warming to room temperature, and crystallization from Et_2O afforded $\text{Ti}(\text{N}_2^{\text{pyr}}\text{N}^{\text{Me}})\{\text{NB}(\text{NAr}'\text{CH})_2\}(\text{py})_2$ (**13**, eq 1) in 34% isolated



yield. The ^1H and ^{13}C NMR spectra of **13** indicate that the complex has C_s symmetry in solution. One set of resonances for the chemically equivalent pyrrolyl groups are observed, whereas two are seen for the chemically inequivalent pyridine ligands (differentiated because of the orientation of the central NMe group of the tridentate ligand). The ^1H and ^{13}C resonances for the borylimido ligand are comparable to those in **8** and **9** and the ^{11}B NMR shows a singlet at 13.2 ppm.

Diffraction-quality crystals of **13** were grown from Et_2O at 5°C . The solid state structure is shown in Figure 4 along with

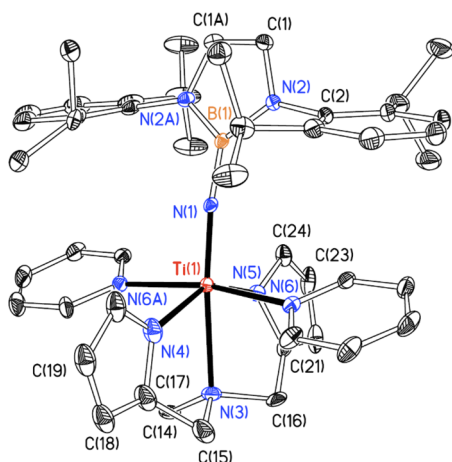


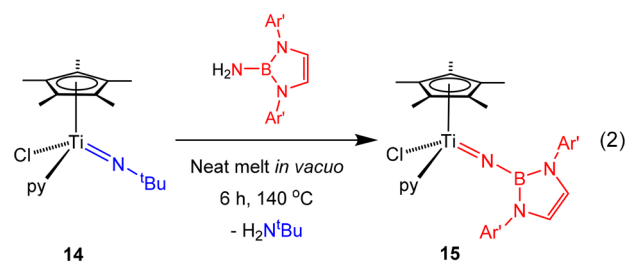
Figure 4. Displacement ellipsoid plot (20% probability) of $\text{Ti}(\text{N}_2\text{pyrNMe})\{\text{NB}(\text{NAr}'\text{CH})_2\}(\text{py})_2$ (**13**). H atoms are omitted for clarity. Atoms carrying the suffix 'A' are related to their counterparts by the symmetry operator $[-x, -y, 1+z]$. Selected bond distances (Å) and angles ($^\circ$): $\text{Ti}(1)-\text{N}(1)$ 1.732(4), $\text{Ti}(1)-\text{N}(3)$ 2.440(5), $\text{Ti}(1)-\text{N}(4)$ 2.064(6), $\text{Ti}(1)-\text{N}(5)$ 2.047(5), $\text{Ti}(1)-\text{N}(6)$ 2.258(3), $\text{N}(1)-\text{B}(1)$ 1.421(8), $\text{N}(1)-\text{Ti}(1)-\text{N}(3)$ 170.6(2), $\text{N}(1)-\text{Ti}(1)-\text{N}(4)$ 114.2(3), $\text{N}(1)-\text{Ti}(1)-\text{N}(5)$ 98.0(2), $\text{N}(1)-\text{Ti}(1)-\text{N}(6)$ 94.67(9), $\text{N}(3)-\text{Ti}(1)-\text{N}(6)$ 85.99(9), $\text{N}(4)-\text{Ti}(1)-\text{N}(5)$ 147.8(3), $\text{N}(4)-\text{Ti}(1)-\text{N}(6)$ 84.76(9), $\text{N}(5)-\text{Ti}(1)-\text{N}(6)$ 92.96(9), $\text{Ti}(1)-\text{N}(1)-\text{B}(1)$ 167.9(4).

selected bond lengths and angles. The tridentate ligand is coordinated in a meridional fashion as part of an overall distorted octahedral geometry, and the borylimido ligand is positioned *trans* to the central NMe donor. The $\text{Ti}(1)-\text{N}(1)$ bond length of 1.732(4) Å is again consistent with a triple bond but longer than that in **9** (1.7118(9) Å) due to the strongly donating anionic pyrrolyl groups. The $\text{N}(1)-\text{B}(1)$ distance of 1.421(8) Å is the same as that in **9** and seems relatively insensitive to the environment at the metal center. The structure also confirms that two pyridine ligands are retained from **9** and possess different environments due to the orientation of C(14).

Synthesis of Half-Sandwich Titanium Borylimides. As mentioned above, half-sandwich *tert*-butylimido, arylimido,

hydrazido, and alkoxyimido complexes have shown a rich reaction chemistry of the $\text{Ti}=\text{NR}$ functional group. The latter three classes have usually been accessed through an imide-amine exchange protocol in which a *tert*-butylimido ligand is displaced as $\text{H}_2\text{N}^t\text{Bu}$ by net protonolysis with the respective aniline, hydrazine, or alkoxyamine.^{3b,24a,28} The only previously reported half-sandwich borylimido compound of any transition metal is $\text{Cp}^*\text{Ti}\{\text{MeC}(\text{N}^i\text{Pr})_2\}(\text{NBC}_8\text{H}_{14})$ (**2**) accessed by reductive $\text{N}_{\text{im}}-\text{NR}_2$ bond cleavage of $\text{Cp}^*\text{Ti}\{\text{MeC}(\text{N}^i\text{Pr})_2\}(\text{NNR}_2)$ ($\text{R} = \text{Me}$ or Ph , *vide supra*). This is not a general route since it works only for 9-BBN.^{4q} In addition it is difficult to separate **2** from the side-product aminoboranes $\text{R}_2\text{NBC}_8\text{H}_{14}$ giving low overall yields. Thus, we aimed to extend the imide-amine methodology to borylimido chemistry using $\text{H}_2\text{NB}(\text{NAr}'\text{CH})_2$ (**6**) and corresponding diorganoborylamines H_2NBR_2 .

When followed on the NMR tube scale in C_6D_6 solution at 90°C , reaction of $\text{Cp}^*\text{Ti}(\text{N}^t\text{Bu})\text{Cl}(\text{py})$ (**14**) with $\text{H}_2\text{NB}(\text{NAr}'\text{CH})_2$ (**6**) resulted in slow and only partial (ca. 10%) conversion to the target borylimido compound **15** at equilibrium. Higher temperatures and removal of the $\text{H}_2\text{N}^t\text{Bu}$ byproduct were required in order to drive the reaction to completion. This was achieved by performing the reaction in the melt, assisted by removal of $\text{H}_2\text{N}^t\text{Bu}$ by a dynamic vacuum. Thus, heating of a mixture of **14** and **6** to 140°C under a dynamic vacuum gave $\text{Cp}^*\text{Ti}\{\text{NB}(\text{NAr}'\text{CH})_2\}\text{Cl}(\text{py})$ (**15**) in 59% isolated yield (eq 2).



As an alternative route to **15**, $\text{Ti}\{\text{NB}(\text{NAr}'\text{CH})_2\}\text{Cl}_2(\text{py})_3$ (**9**) was reacted with 1 equiv of LiCp^* on the NMR tube scale. Heating for 3 days at 70°C in C_6D_6 resulted in conversion of **9** to **15**. However, on scale-up, this route was accompanied by some decomposition side-reactions as judged by formation of $\text{H}_2\text{NB}(\text{NAr}'\text{CH})_2$, which is difficult to separate from **15** due to their similar solubilities. Therefore, only the route *via tert*-butylimide/borylamine exchange was later used to reliably access **15**. Attempts to prepare an unsubstituted cyclopentadienyl (i.e., $\eta\text{-C}_5\text{H}_5$) analogue of **15** from **9** and 1 equiv. NaCp also gave mixtures. This is discussed in further detail later on.

The ^1H and ^{13}C NMR spectra of **15** are consistent with the structure illustrated; a singlet was observed at 15.5 ppm in the ^{11}B NMR spectrum. Diffraction-quality crystals of **15** were grown from a benzene/hexane mixture at room temperature. The solid state structure is shown in Figure 5, along with selected bond distances and angles. The structures of six related complexes of the type $\text{Cp}^*\text{Ti}(\text{NR})\text{Cl}(\text{py})$ ($\text{R} = ^t\text{Bu}$ (**14**), Ar' , 2,6- $\text{C}_6\text{H}_3\text{Br}_2$, 2- $\text{C}_6\text{H}_4^t\text{Bu}$, 2- $\text{C}_6\text{H}_4^i\text{Pr}$, NPh_2) have been reported to date,^{3b,24a,29} all of which are comparable to that of **15** with three-legged piano stool geometries. The $\text{Ti}(1)-\text{N}(1)$ bond distance of 1.7380(11) Å for **15** falls within the range of values found for the arylimido analogues (range 1.7304(19)–1.753(2)

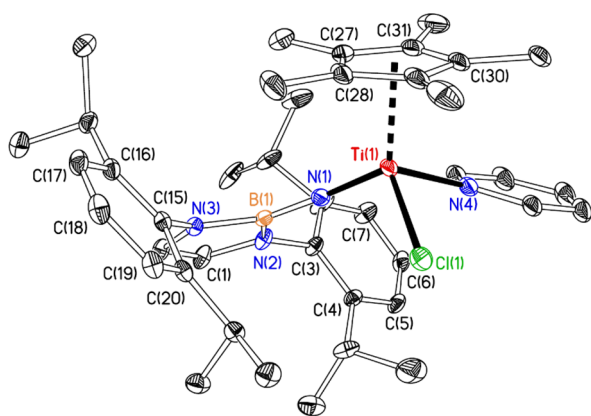


Figure 5. Displacement ellipsoid plot (20% probability) of $\text{Cp}^*\text{Ti}\{\text{NB}(\text{NAr}'\text{CH})_2\}\text{Cl}(\text{py})$ (**15**). H atoms are omitted for clarity. Selected bond distances (Å) and angles ($^\circ$): $\text{Ti}(1)\text{--N}(1)$ 1.7380(11), $\text{Ti}(1)\text{--N}(4)$ 2.1649(11), $\text{Ti}(1)\text{--Cl}(1)$ 2.3212(4), $\text{Ti}(1)\text{--Cp}_{\text{cent}}$ 2.07, $\text{N}(1)\text{--B}(1)$ 1.4153(17), $\text{Cp}_{\text{cent}}\text{--Ti}(1)\text{--N}(1)$ 122.0, $\text{Cp}_{\text{cent}}\text{--Ti}(1)\text{--N}(4)$ 110.1, $\text{Cp}_{\text{cent}}\text{--Ti}(1)\text{--Cl}(1)$ 116.8, $\text{N}(1)\text{--Ti}(1)\text{--Cl}(1)$ 107.68(5), $\text{N}(4)\text{--Ti}(1)\text{--Cl}(1)$ 96.77(4), $\text{N}(1)\text{--Ti}(1)\text{--N}(4)$ 99.16(5), $\text{Ti}(1)\text{--N}(1)\text{--B}(1)$ 175.01(8). Cp_{cent} refers to the centroid for the C_5Me_5 ring carbons.

Å)¹² and is significantly longer than in the *tert*-butylimido homologue (av. 1.697(5) Å).²⁹

In an attempt to access organoborylimides, reactions of $\text{Cp}^*\text{Ti}(\text{N}^t\text{Bu})\text{Cl}(\text{py})$ (**14**) with $\text{H}_2\text{NBC}_8\text{H}_{14}$ and H_2NBMe_2 were also explored. No success was found with either of these substrates, either in solution or melt conditions. At room temperature in C_6D_6 , no reaction was observed with either amine, while the forcing conditions employed in higher temperature solution reactions, or in melts, ultimately resulted only in decomposition products. Further experiments and calculations probing this type of borylamine-*tert*-butylimide exchange reaction are discussed later.

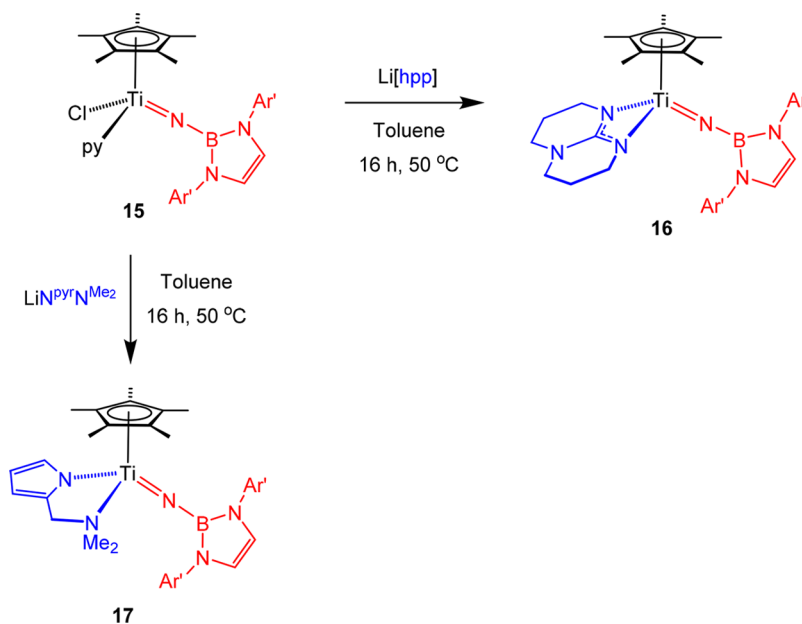
The previously described $\text{Cp}^*\text{Ti}\{\text{MeC}(\text{N}^i\text{Pr})_2\}\{\text{NBC}_8\text{H}_{14}\}$ (**2**)^{4q} is supported by a $\text{Cp}^*/\kappa^2\text{-MeC}(\text{N}^i\text{Pr})_2$ ligand set which

we have found useful as a ligand platform in related compounds.^{4r,6d,8b,30} Attempts to synthesize an analogous compound incorporating the $\text{NB}(\text{NAr}'\text{CH})_2$ ligand by reaction of **15** with either $\text{Li}[\text{MeC}(\text{N}^i\text{Pr})_2]$ or $\text{Li}[\text{PhC}(\text{N}^i\text{Pr})_2]$ failed. This is probably due to significant steric constraints imposed by the large boryl ligand in this case. We therefore turned our attention to alternative monoanionic, $\kappa^2_{\text{N,N}}$ -bidentate ligands with reduced steric profiles. The first of these is the bicyclic guanidinate derived from H-hpp (1,3,4,6,7,8-hexahydro-2H-pyrimido[1,2-*a*]pyrimidine), which has found some application in titanium organoimido chemistry previously.³¹ Second, the aminopyrrolide ligand $\text{N}^{\text{pyr}}\text{N}^{\text{Me}_2}$ ($\text{Me}_2\text{NCH}_2(2\text{-NC}_4\text{H}_3)$) was employed, which, along with related pyrrolide ligands, has been used extensively in Group 4 imido and hydrazido chemistry in recent years.^{4d,e,27a,c,32}

Reaction of **15** with 1 equiv of either $\text{Li}[\text{hpp}]$ or $\text{LiN}^{\text{pyr}}\text{N}^{\text{Me}_2}$ in toluene proceeded smoothly at 50 $^\circ\text{C}$ (Scheme 2). Following workup, $\text{Cp}^*\text{Ti}(\text{hpp})\{\text{NB}(\text{NAr}'\text{CH})_2\}$ (**16**) and $\text{Cp}^*\text{Ti}(\text{N}^{\text{pyr}}\text{N}^{\text{Me}_2})\{\text{NB}(\text{NAr}'\text{CH})_2\}$ (**17**) were isolated in 68 and 71% yield, respectively. The ^1H and ^{13}C NMR spectra of **16** are indicative of a C_s symmetric species. Those of **17** suggest a C_1 symmetric species. The ^{11}B NMR spectra showed single resonances at 14.6 (DFT calculated 14.0) and 15.3 ppm, respectively. Diffraction-quality crystals of **16** and **17** were grown from hexane. The solid state structure of **16** is shown in Figure 6, along with selected bond distances and angles, and that of **17** is shown in Figure S2 of the Supporting Information.

Both **16** and **17** possess three-legged piano stool geometries, with an $\eta^5\text{-C}_5\text{Me}_5$ ligand, η^1 -borylimido ligand and a $\kappa^2\text{-N,N'}$ -hpp or $\text{-N}^{\text{pyr}}\text{N}^{\text{Me}_2}$. Comparison of the metric parameters of the $\text{Ti}\text{--N}_{\text{im}}\text{--B}$ linkages show that the borylimido moiety is broadly similar in the two compounds. The $\text{Ti}(1)\text{--N}(1)$ (1.7433(19) and 1.7444(12) Å in **16** and **17** respectively) and $\text{N}(1)\text{--B}(1)$ distances (1.422(3) and 1.4318(19) Å), along with the $\text{Ti}(1)\text{--N}(1)\text{--B}(1)$ angles (176.00(17) and 174.15(10) $^\circ$) are all in agreement with the structural data discussed above.

Scheme 2. Synthesis of $\text{Cp}^*\text{Ti}(\text{hpp})\{\text{NB}(\text{NAr}'\text{CH})_2\}$ (**16**) and $\text{Cp}^*\text{Ti}(\text{N}^{\text{pyr}}\text{N}^{\text{Me}_2})\{\text{NB}(\text{NAr}'\text{CH})_2\}$ (**17**), from $\text{Cp}^*\text{Ti}\{\text{NB}(\text{NAr}'\text{CH})_2\}\text{Cl}(\text{py})$ (**15**)



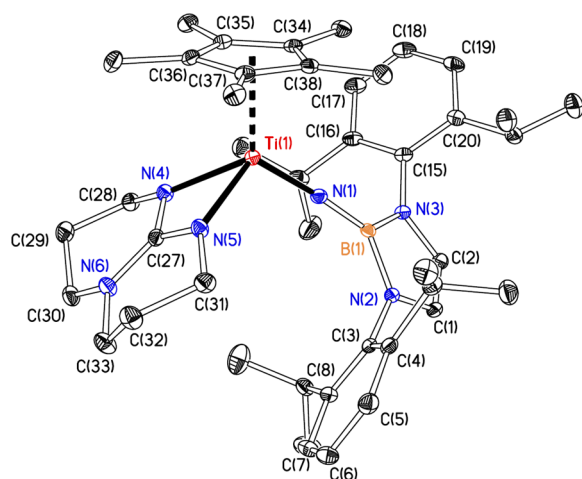


Figure 6. Displacement ellipsoid plot (20% probability) of $\text{Cp}^*\text{Ti}(\text{hpp})\{\text{NB}(\text{NAr}'\text{CH})_2\}$ (**16**). H atoms are omitted for clarity. Selected bond distances (Å) and angles (deg): $\text{Ti}(1)-\text{N}(1)$ 1.7433(19), $\text{Ti}(1)-\text{N}(4)$ 2.0790(18), $\text{Ti}(1)-\text{N}(5)$ 2.0753(19), $\text{Ti}(1)-\text{Cp}_{\text{cent}}$ 2.07, $\text{N}(1)-\text{B}(1)$ 1.422(3), $\text{N}(1)-\text{Ti}(1)-\text{Cp}_{\text{cent}}$ 125.1, $\text{N}(4)-\text{Ti}(1)-\text{Cp}_{\text{cent}}$ 117.1, $\text{N}(5)-\text{Ti}(1)-\text{Cp}_{\text{cent}}$ 115.0, $\text{N}(1)-\text{Ti}(1)-\text{N}(4)$ 109.87(8), $\text{N}(1)-\text{Ti}(1)-\text{N}(5)$ 109.56(8), $\text{N}(4)-\text{Ti}(1)-\text{N}(5)$ 64.95(7), $\text{Ti}(1)-\text{N}(1)-\text{B}(1)$ 176.00(17). Cp_{cent} refers to the centroid for the C_5Me_5 ring carbons.

Compound **16** allows for a fairer comparison (in terms of structural similarity) between its $\text{Ti}-\text{NB}(\text{NAr}'\text{CH})_2$ group and the corresponding $\text{Ti}-\text{NBC}_8\text{H}_{14}$ in $\text{Cp}^*\text{Ti}\{\text{MeC}(\text{N}^i\text{Pr})_2\}-\text{NBC}_8\text{H}_{14}$ (**2**, $\text{Ti}-\text{N}_{\text{im}}$ = 1.731(3) Å).⁴¹ Interestingly, the $\text{Ti}-\text{N}_{\text{im}}$ distances are equivalent (difference = 0.012(4) Å) at the 3σ level of uncertainty, but quite possibly are still influenced by the different steric requirements in each system. The $\text{N}(1)-\text{B}(1)$ distances are also similar (1.422(3) (**16**) and 1.402(4) Å), but the difference of 0.020(5) Å is significant at the 3σ level of uncertainty. This suggests more multiple (π) bond character in the $\text{N}_{\text{im}}-\text{B}$ bond of **2**, as would be expected since the $\text{NBC}_8\text{H}_{14}$ ligand does not have additional N atom (lone pair) donors adjacent to the boron to compete for the vacant 2p atomic orbital. To probe this further we determined the X-ray structure

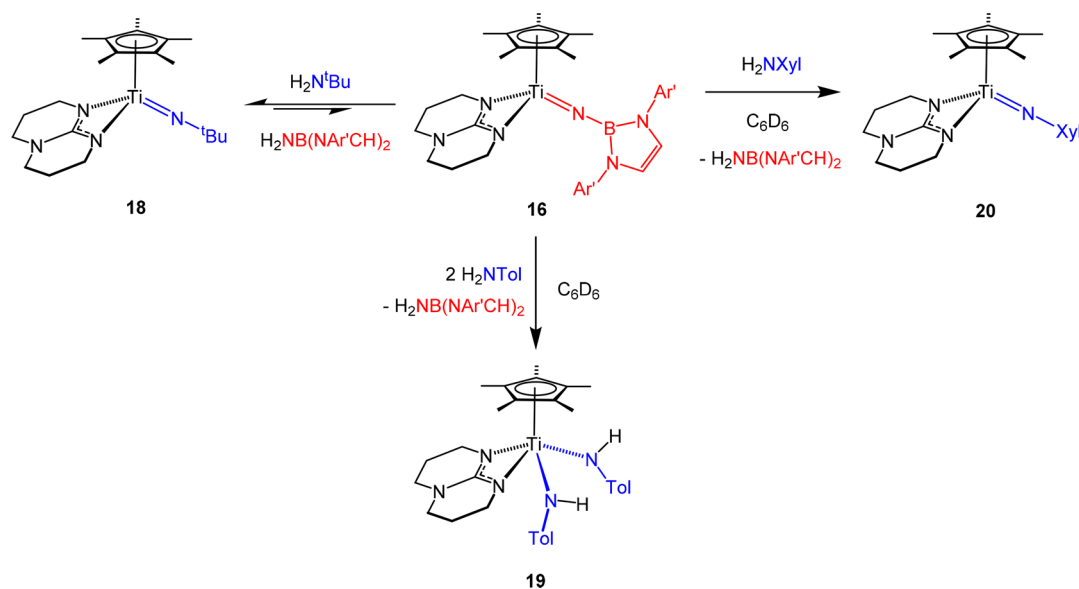
of $\text{H}_2\text{NB}(\text{NAr}'\text{CH})_2$ (see Figure S3 in the Supporting Information) and found a $\text{B}-\text{NH}_2$ distance of 1.41(1) Å (computed value 1.417 Å). The amine “ $\text{H}_2\text{NBC}_8\text{H}_{14}$ ” in fact exists as a $\text{B}(\mu-\text{NH}_2)\text{B}$ bridged dimer in the solid state,³³ so an experimental comparison of the $\text{B}-\text{NH}_2$ distance in the monomer cannot be made. The DFT computed value was 1.395 Å, 0.022 Å shorter than in the computed version of $\text{H}_2\text{NB}(\text{NAr}'\text{CH})_2$. This difference is comparable to that between the $\text{N}(1)-\text{B}(1)$ distances in **16** and **2**. Further comparisons are made using DFT later.

Isodesmic Borylimide-Amine Exchange Reactions. $\text{Cp}^*\text{Ti}(\text{hpp})(\text{N}^t\text{Bu})$ (**18**), the *tert*-butylimido analogue of **16**, was prepared from **14** and $\text{Li}[\text{hpp}]$. Given access to both **16** and **18** independently of each other, these and related hpp-supported compounds were used to develop comparative isodesmic amine-borylimide exchange reactions so as to probe further the bond energetics in these systems (Scheme 3).

The 1:1 reaction of **16** with $\text{H}_2\text{N}^t\text{Bu}$ in C_6D_6 at room temperature immediately formed an equilibrium mixture with **18** and the borylimine **6** (ratio of [**18**]:[**16**] = 70:30; K_{eq} = 5.44) giving an experimental $\Delta_r G$ = −1.0 kcal mol^{−1} at 298 K for the reaction $\text{16} + \text{H}_2\text{N}^t\text{Bu} \rightarrow \text{18} + \text{H}_2\text{NB}(\text{NAr}'\text{CH})_2$. The same equilibrium mixture was formed from the 1:1 reaction of **18** and **6**. DFT calculations gave $\Delta_r G$ = 0.6 kcal mol^{−1}, consistent with a fine-balanced equilibrium.

Reaction of **16** with 1 equiv of H_2NTol gave 50% conversion to the bis(anilido) compound $\text{Cp}^*\text{Ti}(\text{hpp})(\text{NHTol})_2$ (**19**) as opposed to the expected terminal imide $\text{Cp}^*\text{Ti}(\text{hpp})(\text{NTol})$, presumably due to the reduced steric profile of hpp (Scheme 3). Reaction with 2 equiv of H_2NTol quantitatively formed **19**. As a fairer comparison (since formation of **19** is not an isodesmic reaction), the reaction of **16** with 1 equiv of H_2NXyl (Xyl = 2,6- $\text{C}_6\text{H}_3\text{Me}_2$) in C_6D_6 was performed, and this gave quantitative conversion to the terminal imide $\text{Cp}^*\text{Ti}(\text{hpp})(\text{NXyl})$ (**20**) and borylimine **6**. The DFT-computed $\Delta_r G$ for this reaction is −6.1 kcal mol^{−1}, in agreement with experiment. Compounds **19** and **20** were conveniently prepared and fully characterized on scale-up by imide-amine exchange from $\text{Cp}^*\text{Ti}(\text{hpp})(\text{N}^t\text{Bu})$ (**18**) and the respective aniline. The X-

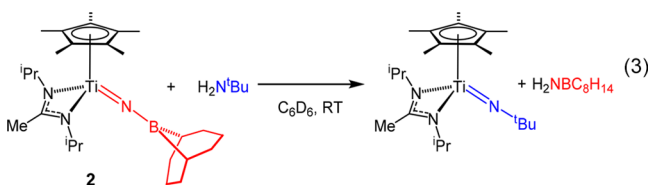
Scheme 3. Borylimido Ligand Exchange Reactions of $\text{Cp}^*\text{Ti}(\text{hpp})\{\text{NB}(\text{NAr}'\text{CH})_2\}$ (**16**) with $\text{H}_2\text{N}^t\text{Bu}$, H_2NXyl , and H_2NTol



ray structures of **18** and **19** are given in Figure S4 of the Supporting Information.

No reaction was observed at room temperature or with heating between $\text{Cp}^*\text{Ti}(\text{hpp})(\text{N}^t\text{Bu})$ (**18**) and either H_2NBMe_2 or $\text{H}_2\text{NBC}_8\text{H}_{14}$ consistent with the failure of other attempts (vide supra) at *tert*-butylimide-amine reactions with these diorganoborylamines. The DFT-computed $\Delta_r G$ for the reaction of **18** with $\text{H}_2\text{NBC}_8\text{H}_{14}$ was $+10.6 \text{ kcal mol}^{-1}$ ($+12.8 \text{ kcal mol}^{-1}$ taking into account initial dissociation of the aminoborane dimer), consistent with experiment. Likewise, $\text{Cp}^*\text{Ti}(\text{hpp})\{\text{NB}(\text{NAr}'\text{CH})_2\}$ (**16**) did not react with either of these aminoboranes.

Since the closely related $\text{Cp}^*\text{Ti}\{\text{MeC}(\text{N}^i\text{Pr})_2\}(\text{NBC}_8\text{H}_{14})$ (**2**) can be prepared without requiring imide-amine or other exchange protocols, it provides an experimental way to probe the energetics of dialkylborylamine-*tert*-butylimide exchange from the opposite direction (eq 3). As expected, reaction of **2**



with 1 equiv of $\text{H}_2\text{N}^t\text{Bu}$ in C_6D_6 quantitatively formed the known²⁸ $\text{Cp}^*\text{Ti}\{\text{MeC}(\text{N}^i\text{Pr})_2\}(\text{N}^t\text{Bu})$ and $\text{H}_2\text{NBC}_8\text{H}_{14}$. The DFT-computed $\Delta_r G$ for this reaction is $-8.2 \text{ kcal mol}^{-1}$ ($-6.0 \text{ kcal mol}^{-1}$ without taking into account dimerization of the aminoborane) at 298 K. Analogous experimental outcomes were found with H_2NTol and H_2NNPh_2 forming $\text{Cp}^*\text{Ti}\{\text{MeC}(\text{N}^i\text{Pr})_2\}(\text{NR})$ ($\text{R} = \text{Tol}$ or NPh_2).^{8b,28,30}

DFT and QTAIM Study of the Bonding and Borylimide-Amine Exchange Energetics of Cyclopentadienyl-Amidinate Complexes. Two previous studies have examined aspects of the bonding in transition metal borylimides, namely, Bettinger's analysis^{16c} of the hypothetical 20 valence electron $(\text{CO})_4\text{Fe}(\text{NBCat})$ and $(\text{CO})_4\text{Fe}(\text{NBH}_2)$, and ours for the transient borylimide $(\text{NacNac}^{\text{NMe}_2})\text{Sc}\{\text{NB}(\text{NAr}'\text{CH})_2\}$ (**7**, Figure 1).¹⁵ We compared scandium-borylimide and scandium-arylimide bonding, concluding that heteroatom-substituted borylimido ligands of the type NB-

$(\text{NAr}'\text{CH})_2$ are better σ - and π -donors than their arylimido counterparts and form stronger $\text{Sc}-\text{N}_{\text{im}}$ bonds. We also accounted for differences observed in the reactions of scandium boryl- and aryl-imido compounds with saturated and unsaturated substrates, concluding that substrate 1,2-addition to the $\text{Sc}-\text{N}_{\text{im}}$ bond of $(\text{NacNac}^{\text{NMe}_2})\text{Sc}(\text{NB}(\text{NAr}'\text{CH})_2)$ is energetically more favorable than the same reaction for $(\text{NacNac}^{\text{NMe}_2})\text{Sc}(\text{NAr}')$. However, these previous studies were necessarily somewhat limited in scope: (i) there are relatively few types of rare earth-imido compounds to compare with, and so a broader contextual view of metal-borylimido bonding could not be developed; (ii) no scandium borylimide has been structurally characterized which prevents the testing of structure-bonding predictions; (iii) no experimental data are available for borylimido compounds $(\text{L})\text{Sc}(\text{NBR}_2)$ without heteroatom donor R-groups. We therefore set out to develop a more detailed and integrated picture of the bonding and thermodynamic features of the different types of borylimides represented by $\text{Cp}^*\text{Ti}\{\text{MeC}(\text{N}^i\text{Pr})_2\}(\text{NBC}_8\text{H}_{14})$ (**2**) and $\text{Cp}^*\text{Ti}(\text{hpp})\{\text{NB}(\text{NAr}'\text{CH})_2\}$ (**16**). We decided to approach this (vide infra) by comparing them with the previously reported alkyl- and aryl-imido, and hydrazido homologues $\text{Cp}^*\text{Ti}\{\text{MeC}(\text{N}^i\text{Pr})_2\}(\text{NR})$ ($\text{R} = ^t\text{Bu}$, aryl, NNR'_2). These have complementary imido N-substituents (no π -effects for $\text{R} = \text{alkyl}$; π -donor for $\text{R} = \text{NR}'_2$; tunable π -acceptor for $\text{R}' = 4-\text{C}_6\text{H}_4\text{X}$ as a function of the *para* X-group).

The DFT complexes used in this study are shown in Figure 7. **1Q_BMe₂** is a model for $\text{Cp}^*\text{Ti}\{\text{MeC}(\text{N}^i\text{Pr})_2\}(\text{NBC}_8\text{H}_{14})$ (**2**), and **1Q_B(NMeCH)₂** represents $\text{Cp}^*\text{Ti}(\text{hpp})\{\text{NB}(\text{NAr}'\text{CH})_2\}$ (**16**). Although the real compound has a κ^2 -guanidinate ligand in place of κ^2 -amidinate, DFT control calculations on the hpp-supported systems $\text{CpTi}(\text{hpp})(\text{NR})$ ($\text{R} = \text{Me}$, Ph , $\text{B}(\text{NMeCH})_2$, BMe_2) showed that their bond dissociation energies and imide-amine exchange energies are very similar to, and scale with, those of their $\text{CpTi}\{\text{MeC}(\text{NMe})_2\}(\text{NR})$ counterparts (Figure S5 of the Supporting Information).

As mentioned, the $\text{Ti}-\text{N}_{\text{im}}$ bonding in alkyl, aryl and hydrazido systems $\text{CpTi}\{\text{MeC}(\text{NMe})_2\}(\text{NR})$ ($\text{R} = \text{Me}$, aryl, NR_2) has been studied previously using molecular orbital and NBO analysis approaches.^{8b} In each case, $\text{Ti}-\text{N}_{\text{im}}$ is described as a triple bond ($\sigma^2\pi^4$ configuration). As a point of reference

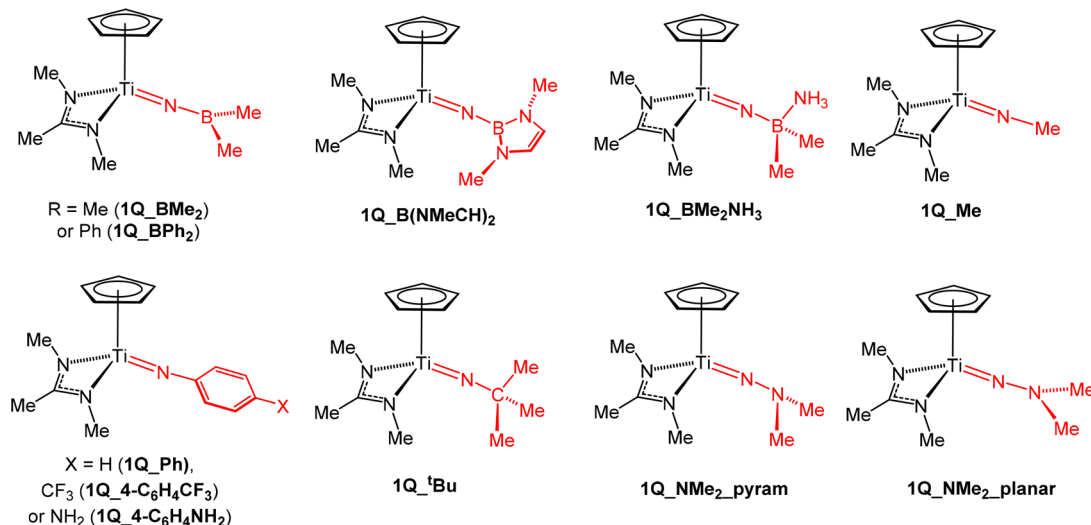


Figure 7. Model cyclopentadienyl-amidinate complexes.

the two Ti–N_{im} π -bonding MOs (denoted π_v (lying in the approximate molecular mirror plane) and π_h) of **1Q Me** are shown in Figure 8. The Ti(3d)–N(2p) component of π_h of

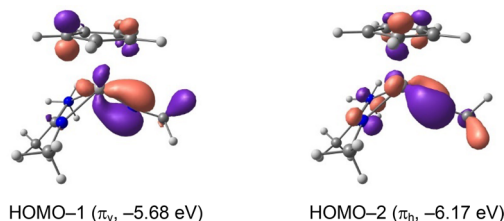


Figure 8. DFT computed Ti–N_{im} π -type molecular orbitals of CpTi{MeC(NMe)₂}(NMe) (**1Q Me**). Isosurfaces are drawn at the 0.036 au contour level.

1Q R does not interact with R-substituent π -type orbitals as they are oriented orthogonal to it, whereas in π_v it interacts quite strongly. When R = phenyl the ring acts as a net π -acceptor from π_v , and where R = NR'₂ it acts as a π -donor to the Ti–N_{im} antibonding MO, π_v^* , especially when the NR'₂ nitrogen is planar as found for R' = Ph.

The different σ - and π -properties of the two types of boryl substituent, BR₂, can be interpreted via the frontier MOs of the corresponding dianions [NBMe₂]^{2–} and [NB(NMeCH)₂]^{2–} (Figure 9). The MOs of [NMe]^{2–} and [NPh]^{2–} computed

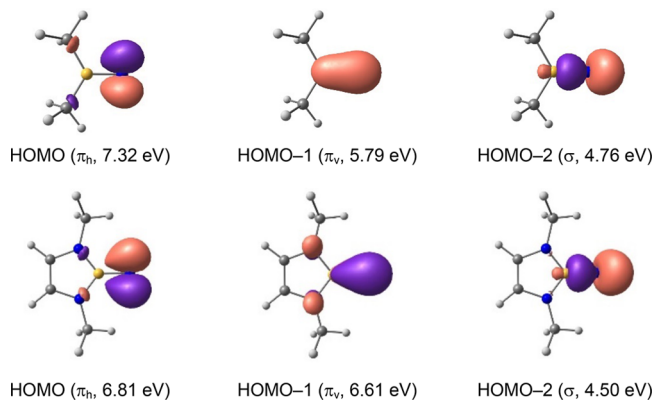


Figure 9. π - and σ -type frontier molecular orbitals of the borylimido dianions [NBMe₂]^{2–} (top) and [NB(NMeCH)₂]^{2–} (bottom) in the geometry of **1Q BMe₂** and **1Q B(NMeCH)₂**. Isosurfaces are drawn at the 0.075 au contour level.

with the same B3PW91/Def2-TZVP methodology are given for comparison in Figure S6 of the Supporting Information. As expected, the π_h and π_v MOs of [NBMe₂]^{2–} have very different energies (Δ = 1.53 eV) due to the N_{im}(2p_v)–B(2p_v) π -interaction. This difference is much smaller in [NPh]^{2–} (Δ = 0.53 eV, Figure S6) and even less in [NB(NMeCH)₂]^{2–} (Δ = 0.30 eV) due to N_{Me}(2p_v)→B(2p_v) donation from the N_{Me} lone pairs. As well as these π -effects from the electronegative N_{Me} substituents, there is also a significant inductive effect which influences the [NBR₂]^{2–} orbital energies. Both the π_h (mainly boron 2p AO character) and σ (boron sp hybrid) MOs of [NB(NMeCH)₂]^{2–} are more stable than in [NBMe₂]^{2–} (Δ = 0.51 and 0.26 eV, respectively).

The Ti–N_{im} π_v and π_h MOs of **1Q BMe₂** and **1Q B(NMeCH)₂** are shown in Figure S7 of the Supporting Information, together with those of **1Q Ph** for comparison. These show the expected general features, with π_h - and π_v -type

Ti–N_{im} MOs being discernible. However, the relatively low symmetry of the complexes, mixing between Ti–Cp and Ti–NBR₂ bonding contributions in the lower energy π_v MOs, and also between the Ti–N_{Me} lone pairs and the Ti–N_{im} π_h interaction prevents us from making more than a qualitative assessment.

In order to gain better insight into the relative bonding capabilities and the imide-amine exchange reactions we used the quantum theory of atoms in molecules (QTAIM)³⁴ method together with computed bond dissociation energies for the metal complexes Cp*Ti{MeC(NMe)₂}(NR) ($\Delta E_{\text{Ti–N(R)}}$) and their corresponding amines H₂NR ($\Delta E_{2\text{H–N(R)}}$), as well as the optimized Ti–N_{im} and N_{im}–R distances. These data are given in Table 1 for the optimized complexes **1Q R**, ordered principally according to the computed Ti–NR bond dissociation energy. Table 2 provides a complementary set of QTAIM and selected NBO data for the same complexes but with Ti–N_{im} fixed at 1.70 Å (**1Q R fxd**) so as to better quantify the variations of QTAIM values with N_{im} R-group alone. Graphical illustrations of the key parameter relationships are given in Figure 10, and Figures S8 and S9 of the Supporting Information.

Bond Length Trends. Comparison of the bond length trends for the Ti–N_{im}–R moiety in the model compounds **1Q R** (Figure 7) with those of the previous and new X-ray structures for Cp*Ti(κ^2 -L^{N₂})(NR) (L^{N₂} = hpp or MeC(NⁱPr)₂) is a means to test the calculations against experiment, as well as probing underlying electronic factors in the absence of steric effects. To aid discussions we consider the variations in the bond lengths $d(\text{Ti–N}_{\text{im}})$ and $d(\text{N}_{\text{im}}\text{–R})$ alongside the respective delocalization indices (δ), ellipticity (ϵ), and net NR group charges ($Q(\text{NR})$) from the QTAIM analysis. $\delta(\text{A–B})$ for a bond pair “A–B” is the number of electron pairs shared between the atoms, and is a measure of bond order for the same atomic types. The ellipticity measures the extent to which electron density is differentially accumulated in a given plane containing the bond path, and is 0 for a cylindrically symmetric bond.

The trends in $d(\text{Ti–N}_{\text{im}})$ and their approximate values for the model imides and hydrazides (R = Me, Ar, NMe₂) follow that found previously by experiment.¹⁹ The increasing magnitude of $d(\text{Ti–N}_{\text{im}})$, $\delta(\text{N}_{\text{im}}\text{–R})$ and ϵ , and decreasing $d(\text{N}_{\text{im}}\text{–R})$, $\delta(\text{Ti–N}_{\text{im}})$, and $Q(\text{NR})$, in the order R = Me, 4-C₆H₄NH₂, Ph, 4-C₆H₄CF₃ tracks the changes in delocalization of the π_v component of the Ti–N_{im} bond to the aryl ring. The corresponding changes in these values from **1Q NMe₂ pyram** to **1Q NMe₂ planar** (e.g., increase in ϵ and $d(\text{Ti–N}_{\text{im}})$ and decrease in $\delta(\text{Ti–N}_{\text{im}})$) reflect increased lone pair donation from N_β to π_v^* of the Ti–N_{im} bond in orbital terms.

The Ti–N_{im} distance for **1Q BMe₂** (1.706 Å) is between that of **1Q Ph** (1.702 Å) and **1Q 4-C₆H₄CF₃** (1.708 Å), and longer than in **1Q Me** (1.679 Å). This is in agreement with the X-ray data for Cp*Ti{MeC(NⁱPr)₂}(NBC₈H₁₄) (**2**), Cp*Ti{MeC(NⁱPr)₂}(NXyl)²⁸ and Cp*Ti(hpp)(NⁱBu) (**18**) (Ti–N_{im} = 1.731(3), 1.738(1), and 1.7081(18) Å, respectively). The models find also that $d(\text{Ti–N}_{\text{im}})$ is slightly shorter for **1Q B(NMeCH)₂**, whereas $d(\text{Ti–N}_{\text{im}})$ in Cp*Ti(hpp){NB(NAr'CH)₂} (**16**, 1.7433(19) Å) is comparable within error to that in **2** and Cp*Ti{MeC(NⁱPr)₂}(NXyl), presumably reflecting the large steric profile of the real NB(NAr'CH)₂ ligand in **16**. Addition of NH₃ to the boron atom of **1Q BMe₂** gives the hypothetical **1Q BMe₂NH₃** ($d(\text{Ti–N}_{\text{im}})$ = 1.674 Å) with a formally sp³ hybridized boron and no 2p_v π -acceptor

Table 1. Data for Optimized CpTi[MeC(NMe)₂](NR) (1Q_R; R = NMe₂, B(NMeCH)₂, BMe₂NH₃, Me, 4-C₆H₄CF₃, Ph, 4-C₆H₄NH₂, NMe₂ (pyramidal and planar N_B))^a

compound	d(Ti–N _{im}) (Å)	d(N _{im} –R) (Å)	δ(Ti–N _{im})	δ(N _{im} –R)	ε(Ti–N _{im})	ρ(Ti–N _{im})	∇ ² ρ(Ti–N _{im})	Q(NR)	ΔE _{Ti–N(R)} (kcal mol ^{–1})	ΔE _{2H–N(R)} (kcal mol ^{–1})	ΔE _{exch} (kcal mol ^{–1})
1Q_BMe ₂	1.706	1.415	1.590	0.535	0.211	0.206	0.712	–0.887	132.3	225.8	11.7
1Q_B(NMeCH) ₂	1.694	1.429	1.632	0.482	0.063	0.212	0.727	–0.851	119.6	202.3	0.8
1Q_BMe ₂ NH ₃	1.674	1.504	1.772	0.407	0.032	0.222	0.765	–0.747	117.2	204.7	5.7
1Q_Me	1.679	1.417	1.673	1.046	0.091	0.209	0.819	–0.802	109.7	191.5	0.0
1Q_4-C ₆ H ₄ CF ₃	1.708	1.361	1.498	1.128	0.152	0.196	0.770	–0.912	111.6	191.0	–2.4
1Q_Ph	1.702	1.366	1.534	1.112	0.134	0.199	0.780	–0.874	108.2	188.2	–1.8
1Q_4-C ₆ H ₄ NH ₂	1.700	1.369	1.550	1.107	0.110	0.200	0.781	–0.838	103.3	182.4	–2.8
1Q_NMe ₂ _pyram	1.699	1.346	1.551	1.287	0.041	0.193	0.811	–0.749	94.6	170.0	–6.5
1Q_NMe ₂ _planar	1.712	1.320	1.501	1.351	0.210	0.182	0.841	–0.695	93.3	168.1	–7.0
1Q_‘Bu	1.681	1.436	1.665	0.956	0.059	0.207	0.832	–0.806	109.4	192.8	1.6

^a(i) Ti–N_{im} and N_{im}–R bond distances (d); (ii) QTAIM data (atomic units) at the bond critical points: δ(A–B) (delocalization index for the A₂B pair), ε (electron density), ∇²ρ (electron density Laplacian) and Q(NR) (sum of the NR atomic charges); (iii) Ti–N_{im} bond dissociation energy (ΔE_{Ti–N(R)}), complete N–H bond dissociation (ΔE_{2H–N(R)}) and imide-amine exchange energy (ΔE_{exch}), all as defined in Scheme 4.

orbital. For comparison, we also computed the isoelectronic and isosteric 1Q_‘Bu, which has $d(\text{Ti–N}_{\text{im}}) = 1.681 \text{ \AA}$, similar to that of 1Q_Me and 1Q_BMe₂NH₃.

The decrease in $d(\text{Ti–N}_{\text{im}})$ and corresponding increase in $d(\text{N}_{\text{im}}\text{–B})$ from 1Q_BMe₂ to 1Q_B(NMeCH)₂ and then to 1Q_BMe₂NH₃ parallels the changing π -acceptor character of boron. The QTAIM data allow a quantitative evaluation of the relative π -effects. For example, ϵ for Ti–N_{im} in 1Q_BMe₂ (0.211) is larger even than for 1Q_4-C₆H₄CF₃ (0.152), and much larger than in 1Q_B(NMeCH)₂ (0.063). This ϵ is comparable to that in 1Q_BMe₂NH₃ ($\Delta = 0.032$) whose boron atom has no 2p_y π -acceptor orbital. The changes in the magnitudes of $d(\text{Ti–N}_{\text{im}})$, $\delta(\text{Ti–N}_{\text{im}})$ and $Q(\text{NR})$ from 1Q_BMe₂ to 1Q_BMe₂NH₃ ($\Delta = 0.032 \text{ \AA}$, 0.182 and 0.140 e) are all significantly larger than from the isoelectronic 1Q_Ph to 1Q_‘Bu ($\Delta = 0.021 \text{ \AA}$, 0.010 and 0.068 e). These QTAIM and metric data confirm that the BMe₂ N_{im}-substituent (and dialkyl- or diaryl-boron in general) is a much better π -acceptor than a phenyl group, whereas the B(NMeCH)₂ group (or its real homologues) is a less good acceptor even than an electron-rich aryl group as modeled by 1Q_4-C₆H₄NH₂.

The data in Table 1 for the fully optimized 1Q_R show that $d(\text{Ti–N}_{\text{im}})$ and $\delta(\text{Ti–N}_{\text{im}})$ are strongly correlated ($R^2 = 0.866$, cf. Figure S8a in the Supporting Information). We also found that the Ti–N_{im} bonds of 1Q_R have a shallow potential energy surface. In a linear transit calculation, we found that $d(\text{Ti–N}_{\text{im}})$ for 1Q_Me could be extended by ca. 0.04 Å from its equilibrium value of 1.679 to 1.720 Å (longer than any other 1Q_R $d(\text{Ti–N}_{\text{im}})$ value) at a cost of only 0.25 kcal mol^{–1} (and by up to 1.75 Å with $\Delta E = 1.24 \text{ kcal mol}^{-1}$). The QTAIM parameters also change with $d(\text{Ti–N}_{\text{im}})$. For example, δ decreased from 1.673 to 1.629 and ϵ increased from 0.091 to 0.111 on increasing $d(\text{Ti–N}_{\text{im}})$ for 1Q_Me to 1.720. In order to compare the QTAIM data for 1Q_R without the secondary effects from bond length changes we recalculated all of the systems with a fixed Ti–N_{im} bond length of 1.70 Å (median value). These results are shown in Table 2 for the model compounds labeled 1Q_R_fixd and correlate well with the those for 1Q_R. Gratifyingly, we found that the $d(\text{Ti–N}_{\text{im}})$ values in optimized 1Q_R correlated well ($R^2 = 0.823$) with the $\delta(\text{Ti–N}_{\text{im}})$ values in the fixed Ti–N_{im} bond distance series, 1Q_R_fixd as shown in Figure S8b. In most of the further discussions below we will refer to the 1Q_R_fixd QTAIM parameters in order to extract cleanly the electronic effects of the various imide R-substituents.

Bond Energies and Imide-Amine Exchange Energetics.

The calculations for 1Q_R are consistent with Ti–N_{im} bond lengths (and bond order as judged by $\delta(\text{Ti–N}_{\text{im}})$) being strongly influenced by the π -donor or π -acceptor ability of the N_{im} substituent.^{8b,17a,35} On the other hand, lengthening $d(\text{Ti–N}_{\text{im}})$ in 1Q_Me by over 0.07 Å destabilized the compound only ca. 1.2 kcal mol^{–1}, suggesting that Ti–N_{im} bond distance or bond order *per se* may not be reliable indicators of overall Ti–N_{im} bond strength. The well-behaved isodesmic imide-amine exchange reactions described above (Scheme 3 and eq 3) in principle provide experimental insight into the relative bond energetics of these imido and hydrazido compounds. We therefore computed (Table 1) the Ti–N_{im} bond dissociation energies ($\Delta E_{\text{Ti–N(R)}}$) for 1Q_R, as well as for the 2 × H–N bond dissociation process $\text{H}_2\text{NR} \rightarrow 2 \text{ H} + \text{NR}$ ($\Delta E_{2\text{H–N(R)}}$) for the corresponding amines.

Table 1 shows that $\Delta E_{\text{Ti–N(R)}}$ increases generally in the order R = NMe₂ < aryl < Me < BR₂. There is no significant

Table 2. Data for $\text{CpTi}\{\text{MeC}(\text{NMe})_2\}(\text{NR})$ with $\text{Ti}-\text{N}_{\text{im}}$ Fixed at 1.70 Å (1Q_R_fxd ; $\text{R} = \text{BMe}_2, \text{B}(\text{NMeCH})_2, \text{BMe}_2\text{NH}_3, \text{Me}, 4\text{-C}_6\text{H}_4\text{CF}_3, \text{Ph}, 4\text{-C}_6\text{H}_4\text{NH}_2, \text{NMe}_2$ (Pyramidal and Planar N_β))^a

compound	δ	ϵ	ρ	$\nabla^2\rho$	H	G/ρ	%Ti in σ NLMO	sp^x of σ NLMO	%Ti in π_h NLMO	%Ti in π_v NLMO
$1\text{Q_BMe}_2\text{_fxd}$	1.596	0.208	0.210	0.719	−0.114	1.400	20.4	1.94	30.2	17.2
$1\text{Q_B}(\text{NMeCH})_2\text{_fxd}$	1.627	0.063	0.209	0.722	−0.113	1.405	19.4	1.53	26.1	25.7
$1\text{Q_BMe}_2\text{NH}_3\text{_fxd}$	1.749	0.032	0.208	0.740	−0.112	1.428	20.3	1.05	25.8	30.0
1Q_Me_fxd	1.653	0.096	0.199	0.793	−0.101	1.508	18.0	0.64	28.7	29.1
$1\text{Q_4-C}_6\text{H}_4\text{CF}_3\text{_fxd}$	1.506	0.150	0.200	0.780	−0.103	1.490	17.4	0.83	27.1	24.6
1Q_Ph_fxd	1.536	0.133	0.200	0.783	−0.103	1.494	17.6	0.81	27.4	25.8
$1\text{Q_4-C}_6\text{H}_4\text{NH}_2\text{_fxd}$	1.549	0.111	0.200	0.781	−0.103	1.491	17.5	0.78	27.1	26.9
$1\text{Q_NMe}_2\text{_pyram_fxd}$	1.550	0.041	0.192	0.809	−0.095	1.545	17.0	0.45	25.2	34.1
$1\text{Q_NMe}_2\text{_planar_fxd}$	1.515	0.205	0.188	0.859	−0.089	1.618	16.7	0.51	22.9	37.2

^a(i) QTAIM data (atomic units) at the $\text{Ti}-\text{N}_{\text{im}}$ bond critical points: δ (delocalization index), ϵ (ellipticity), ρ (electron density), $\nabla^2\rho$ (electron density Laplacian), H (total energy density) and G/ρ (G = kinetic energy density). (ii) Percentage Ti participation (%Ti) in the stated $\text{Ti}-\text{N}_{\text{im}}$ NLMOs, and proportion of N_{im} 2p character x in the sp^x hybrid orbital used to form the $\text{Ti}-\text{N}_{\text{im}}$ σ -bond, as obtained from NBO calculations.

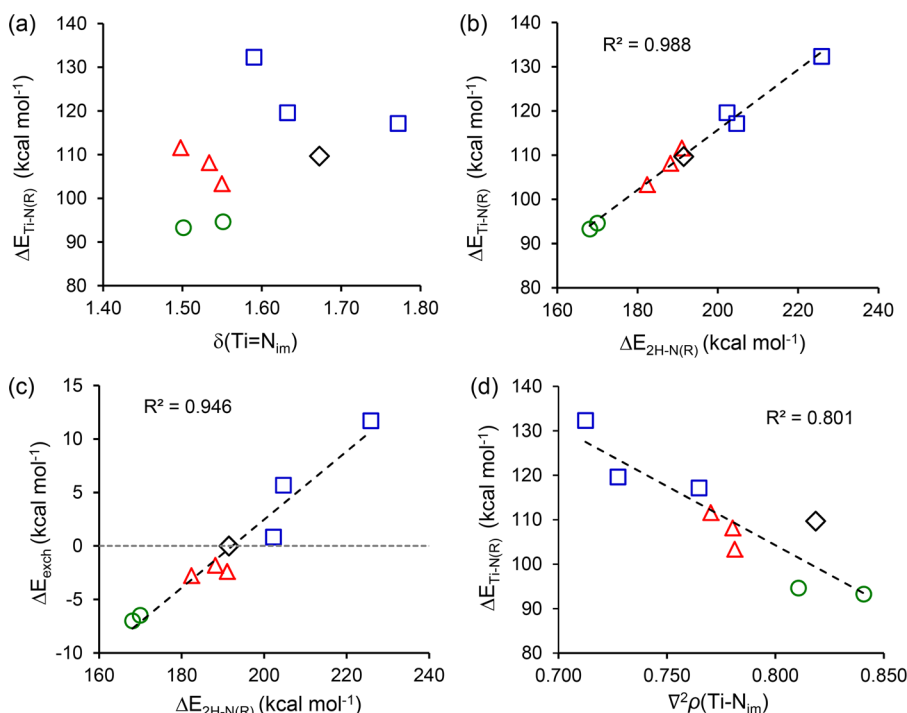
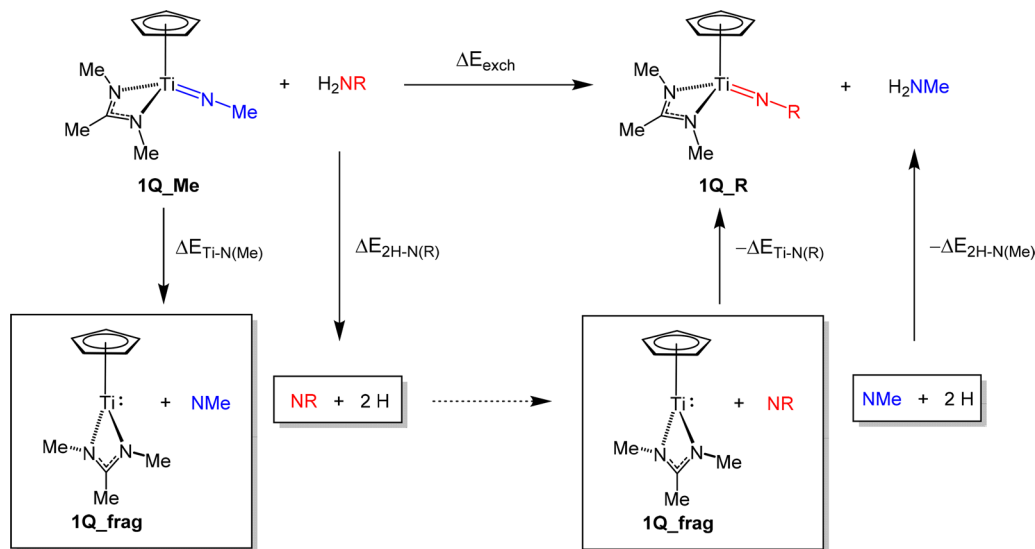


Figure 10. (a) Plot of $\Delta E_{\text{Ti-N(R)}}$ for $\text{CpTi}\{\text{MeC}(\text{NMe})_2\}(\text{NR})$ (1Q_R) vs. $\delta(\text{Ti}-\text{N}_{\text{im}})$. (b) Plot of $\Delta E_{\text{Ti-N(R)}}$ for $\text{CpTi}\{\text{MeC}(\text{NMe})_2\}(\text{NR})$ (1Q_R) vs. $\Delta E_{2\text{H-N(R)}}$ for H_2NR . (c) Plot of ΔE_{exch} vs. $\Delta E_{2\text{H-N(R)}}$. (d) Plot of $\Delta E_{\text{Ti-N(R)}}$ for $\text{CpTi}\{\text{MeC}(\text{NMe})_2\}(\text{NR})$ (1Q_R) vs. $\nabla^2\rho(\text{Ti}-\text{N}_{\text{im}})$. Key for all plots: blue squares, $\text{R} = \text{BMe}_2, \text{B}(\text{NMeCH})_2, \text{BMe}_2\text{NH}_3$; black diamond, $\text{R} = \text{Me}$; red triangles, $\text{R} = 4\text{-C}_6\text{H}_4\text{CF}_3, \text{Ph}, 4\text{-C}_6\text{H}_4\text{NH}_2$; green circles, $\text{R} = \text{NMe}_2$ (pyramidal and planar N_β).

correlation ($R^2 \approx 0.2$) between $\Delta E_{\text{Ti-N(R)}}$ and either $d(\text{Ti}-\text{N}_{\text{im}})$ or $\delta(\text{Ti}-\text{N}_{\text{im}})$ (Figure 10a) across the full range of compounds. In contrast, $\Delta E_{\text{Ti-N(R)}}$ for $\text{CpTi}\{\text{MeC}(\text{NMe})_2\}(\text{NR})$ (1Q_R) correlates very strongly with $\Delta E_{2\text{H-N(R)}}$ for H_2NR ($R^2 = 0.988$). Figure 10b shows this relationship graphically. The gradient of the linear fit to the data from regression analysis is 0.32(3) showing that while both $\Delta E_{\text{Ti-N(R)}}$ and $\Delta E_{2\text{H-N(R)}}$ increase in the same way with changing R -substituent, $\Delta E_{2\text{H-N(R)}}$ increases faster.

The thermodynamic cycle in Scheme 4 allows the SCF energy (ΔE_{exch}) of imide-amine exchange to be calculated from the individual $\Delta E_{\text{Ti-N(R)}}$ and $\Delta E_{2\text{H-N(R)}}$ data, which can then be tested against experiment. Figure 10c illustrates the strong linear relationship ($R^2 = 0.946$) between ΔE_{exch} and $\Delta E_{2\text{H-N(R)}}$. There is a similar relationship with $\Delta E_{\text{Ti-N(R)}}$ ($R^2 = 0.886$) but none with $d(\text{Ti}-\text{N}_{\text{im}})$ ($R^2 = 0.09$), for example. The horizontal line in Figure 10c intercepting the ordinate axis at $\Delta E_{\text{exch}} = 0.0$

represents the thermoneutral exchange between $(\text{L})\text{Ti}=\text{NMe}$ and H_2NMe . Setting aside steric factors or kinetic limitations, and assuming $\Delta_r S$ is relatively insignificant, any points which lie below the horizontal line represent electronically favorable reactions, while those above are unfavorable. The data match known experimental data well: titanium alkylimido ligands are readily substituted by anilines and hydrazines.^{1c,e,4r,8b} Within the arylimido systems alone, anilines with electron-withdrawing groups displace less electron-deficient arylimides³⁵ (cf. $\Delta E_{\text{exch}} = -0.58 \text{ kcal mol}^{-1}$ ($K_{\text{eq}} = 2.8$) for $1\text{Q_Ph} + \text{H}_2\text{N-4-C}_6\text{H}_4\text{CF}_3 \rightarrow 1\text{Q_4-C}_6\text{H}_4\text{CF}_3 + \text{H}_2\text{NPh}$). The DFT results are consistent with the borylimido results summarized in Scheme 3 and eq 3. Reaction of $\text{Cp}^*\text{Ti}(\text{hpp})\{\text{NB}(\text{NAr}'\text{CH}_2)_2\}$ (16) with $\text{H}_2\text{N}^t\text{Bu}$ formed an equilibrium mixture with $\text{Cp}^*\text{Ti}(\text{hpp})(\text{N}^t\text{Bu})$ (18) and borylamine 6 with experimental $\Delta_r G = -1.0 \text{ kcal mol}^{-1}$. Similarly, $\Delta E_{\text{exch}} = -0.83 \text{ kcal mol}^{-1}$ for $1\text{Q_B}(\text{NMeCH})_2 + \text{H}_2\text{NMe} \rightarrow 1\text{Q_Me} + \text{H}_2\text{NB}(\text{NMeCH})_2$. The reaction between

Scheme 4. SCF Energy Decomposition Scheme for the Isodesmic Exchange Reactions of **1Q_Me** with amines H_2NR^a 

^a $\Delta E_{\text{exch}} = \Delta E_{\text{Ti-N(Me)}} + \Delta E_{2\text{H-N(R)}} - \Delta E_{\text{Ti-N(R)}} - \Delta E_{2\text{H-N(Me)}}$. All fragments are in their relaxed geometries for an $S = 1$ spin state except for H ($S = 1/2$).

$\text{Cp}^*\text{Ti}\{\text{MeC}(\text{N}^i\text{Pr})_2\}(\text{NBC}_8\text{H}_{14})$ and $\text{H}_2\text{N}^t\text{Bu}$ is quantitative in favor of $\text{Cp}^*\text{Ti}\{\text{MeC}(\text{N}^i\text{Pr})_2\}(\text{N}^t\text{Bu})$ (eq 3), while $\Delta E_{\text{exch}} = -11.7 \text{ kcal mol}^{-1}$ for $\mathbf{1Q_BMe}_2 + \text{H}_2\text{NMe} \rightarrow \mathbf{1Q_Me} + \text{H}_2\text{NBMe}_2$.

Bond Energies and QTAIM Parameters. To gain a better understanding of the computed trends in Ti– N_{im} bond energies, we turned again to the QTAIM data. Specifically, the signs and magnitude of the electron density (ρ), its Laplacian ($\nabla^2\rho$) and the total energy density (H) at the bond critical point of a bond “A–B” can all give indications of A–B bond strengths. Table 1 gives $\nabla^2\rho$ data for the optimized **1Q_R** systems, and Table 2 provides a wider set of QTAIM parameters for the **1Q_R_fxd** series where we separate out the electronic effects of the imido R-group from small perturbations with changing $d(\text{Ti}–\text{N}_{\text{im}})$. The values of G/ρ (G = kinetic energy density), which can relate to bond polarity, are also listed in Table 2.

In general, the magnitudes of ρ and H at the bond critical points, and the positive value of the electron density Laplacian ($\nabla^2\rho$) are consistent with the expected polar, covalent Ti– N_{im} bonds in **1Q_R** and **1Q_R_fxd**. Figure 10d illustrates the linear negative relationship ($R^2 = 0.801$) between $\Delta E_{\text{Ti-N(R)}}$ and $\nabla^2\rho$ for **1Q_R**; the corresponding plot for **1Q_R_fxd** (Figure S9a) has $R^2 = 0.834$. $\nabla^2\rho$ is a measure of the concentration of electron density at the bond critical point (BCP). A more negative value of $\nabla^2\rho$ indicates a higher degree of covalency for a homologous series of compounds. $\nabla^2\rho$ is in fact the sum of three curvatures of electron density (λ_n , $n = 1, 2, 3$) at the BCP. Table S1 of the Supporting Information gives the breakdown for these values for **1Q_R_fxd**. λ_1 and λ_2 reflect the concentration of electron density along the bond path. They are negative for all **1Q_R_fxd**, and become increasingly negative with $\Delta E_{\text{Ti-N(R)}}$ (av. $R^2 = 0.878$). Furthermore, the values of ρ , H , and G/ρ (Table S2, Figure S9) all correlate with $\Delta E_{\text{Ti-N(R)}}$ ($R^2 = 0.839$ – 0.874) in a way that points to increasing covalency and bond strength, and decreasing Ti– N_{im} polarity, in the order $\text{R} = \text{NMe}_2$ (least covalent) < aryl < Me < BR_2 (most covalent), regardless of $d(\text{Ti}–\text{N}_{\text{im}})$ or $\delta(\text{Ti}–\text{N}_{\text{im}})$.

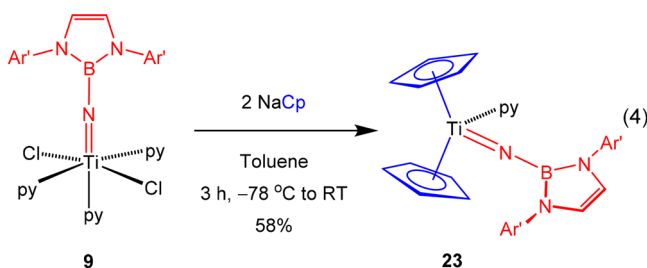
To relate these results back to orbital interpretations we analyzed the electronic structures of **1Q_R_fxd** using the NBO method.^{7,36} This approach aids interpretation of the bonding in terms of idealized Lewis structures. The NBO calculations were set up with the σ - and π -donor NBOs of N_{im} described formally as lone pairs donating to acceptor NBOs on titanium, ultimately forming the σ -, π_h -, and π_v -NLMOs of the Ti– N_{im} triple bonds (NLMO = natural localized MO). The NLMOs of **1Q_BMe}_2_fxd are shown by way of example in Figure S10 of the Supporting Information.**

Table 2 gives the extent of Ti participation (expressed as %Ti orbital character) in these various NLMOs, and the proportion of N_{im} atom 2p character x in the sp^x hybrid donor orbital contributing to the Ti– N_{im} σ -bond. The %Ti in the σ and π_h NLMOs increases with Ti– N_{im} bond covalency as judged by negative correlations with $\nabla^2\rho$ (larger %Ti for less positive $\nabla^2\rho$). The degree of N_{im} 2p character also increases significantly with decreasing $\nabla^2\rho$. For example, the σ -bond for **1Q_BMe}_2_fxd is formed using a $\text{sp}^{1.6}$ -hybridized N_{im} hybrid, whereas that for **1Q_NMe}_2_{\text{planar_fxd}} is formed with a $\text{sp}^{0.51}$ N_{im} hybrid orbital (Bent’s rule³⁷ predicts that N_{im} 2s character would accumulate preferentially toward more electropositive R-group bond partners). The increased N_{im} 2p character in the σ -bonding NBO has the effect of polarizing this donor orbital toward Ti, improving the σ -donor ability of NR. The bond dissociation energies $\Delta E_{\text{Ti-N(R)}}$ scale linearly with % Ti in the σ - and π_h -donor NLMOs and with the x value of sp^x (Figures S9e ($R^2 = 0.798$) and S9f ($R^2 = 0.859$)).****

Whereas %Ti generally increases in the σ - and π_h -NLMO from **1Q_NMe}_2_{\text{planar_fxd}} to **1Q_BMe}_2_fxd, the position for the π_v -NLMO is different and is dominated by the π -bonding character of R. %Ti decreases substantially from **1Q_B(NMeCH)}_2_fxd (25.7) to **1Q_BMe}_2_fxd (17.2%), and slightly from **1Q_4-C}_6\text{H}_4\text{NH}_2_fxd (26.9%) to **1Q_4-C}_6\text{H}_4\text{CF}_3_fxd (24.6%) as expected, showing that π_v becomes more ligand-based. Analogously, %Ti increases from **1Q_NMe}_2_{\text{pyram_fxd}}** (34.1%) to **1Q_NMe}_2_{\text{planar_fxd}}** (37.1%). Overall there is a negative correlation ($R^2 = 0.873$) between $\Delta E_{\text{Ti-N(R)}}$ and %Ti (and a modest positive correlation************

($R^2 = 0.774$) between $\nabla^2\rho$ and %Ti) for those **1Q_R** planar **fxd** systems which have significant R-group π -character. This reflects the Ti–N_{im} bond weakening effect of both π -acceptor and π -donor N_{im} substituents.

Synthesis and Structures of Bis(cyclopentadienyl) titanium Borylimido Compounds. A wide range of metal–ligand multiply bonded Group 4 metallocenes of the type $\text{Cp}^R_2\text{M(E)(L)}$ (M = Ti, Zr, Hf; E = NR, PR, O, S, Se, Te; L = Lewis base) have been previously reported.^{2a,3h,38} These are interesting, both in terms of reactivity and of their electronic structure, being so-called “ π -loaded” (formally 20 valence electron) compounds. We have previously shown that both the *tert*-butylimide $\text{Cp}_2\text{Ti}(\text{N}^t\text{Bu})(\text{py})$ (**21**) and diphenylhydrazide $\text{Cp}_2\text{Ti}(\text{NNPh}_2)(\text{py})$ (**22**) can be prepared from the respective $\text{Ti}(\text{NR})\text{Cl}_2(\text{py})_3$ precursor (R = ^tBu or NPh₂).^{3h,38a} Gratifyingly, reaction of $\text{Ti}\{\text{NB}(\text{NAr}'\text{CH})_2\}\text{Cl}_2(\text{py})_3$ (**9**) with two equiv of NaCp formed the corresponding titanocene borylimide $\text{Cp}_2\text{Ti}\{\text{NB}(\text{NAr}'\text{CH})_2\}(\text{py})$ (**23**) in 58% isolated yield (eq 4). The ¹H and ¹³C NMR spectra of **23** are consistent



with the proposed structure, and the borylimido ligand gave a singlet at 18.0 ppm in the ¹¹B NMR spectrum, consistent with all the other borylimides of this type discussed above. As mentioned, the reaction of **9** with 1 equiv of NaCp did not cleanly form the target half-sandwich compound $\text{CpTi}\{\text{NB}(\text{NAr}'\text{CH})_2\}\text{Cl}(\text{py})$ (**24**). However, we were able to prepare **24** through a redistribution reaction between **9** and **23** at 70 °C over 5 days. Full details are provided in the [Supporting Information](#).

Diffraction-quality crystals of **23** were grown from pentane at 5 °C. The solid state structure is shown in [Figure 11](#), along with selected bond distances and angles. Molecules of **23** contain a bent Cp_2Ti moiety which is coordinated to both the borylimido ligand and a pyridine donor ligand. Although this is the first borylimido sandwich compound of any metal, its structure may be compared to other Group 4 metallocenes of the type $\text{Cp}^R_2\text{M(E)(L)}$. The Cp rings of **23** are best described as η^5 -coordinated to the metal with Ti–C bonds in the range 2.4022(18)–2.6053(18) Å, and an average Ti–Cp_{cent} distance of 2.18 ± 0.04 Å (av. of 2.14 and 2.22 Å). These values are comparable to those in the analogous *tert*-butylimide $\text{Cp}_2\text{Ti}(\text{N}^t\text{Bu})(\text{py})$ (**21**, av. 2.22 Å) and hydrazide $\text{Cp}_2\text{Ti}(\text{NNPh}_2)(\text{py})$ (**22**, av. 2.18 Å).^{3h,38a} They are, however, ca. 0.1 Å longer than the Ti–Cp_{cent} distances generally found in titanocene complexes of the type $\text{Cp}^R_2\text{TiX}_2$ (X = Cl, alkyl),¹⁹ because of the π -loaded nature of these compounds. The “upper” Cp ring (as drawn in [Figure 11](#)) of **23** has a noticeable ring-slip toward η^3 -coordination (Ti(1)–C(28) and Ti(1)–C(29) = 2.6050(18) and 2.6053(18) Å, respectively), whereas all of the other Ti–C lengths in this and the “lower” Cp ring are in the range ca. 2.402–2.503 Å. The Ti(1)–N(1) bond length of 1.7549(13) Å and Cp_{cent}–Ti–Cp_{cent} angle of 125.1° is comparable to the Ti–N_{im} distance in the hydrazide **22**

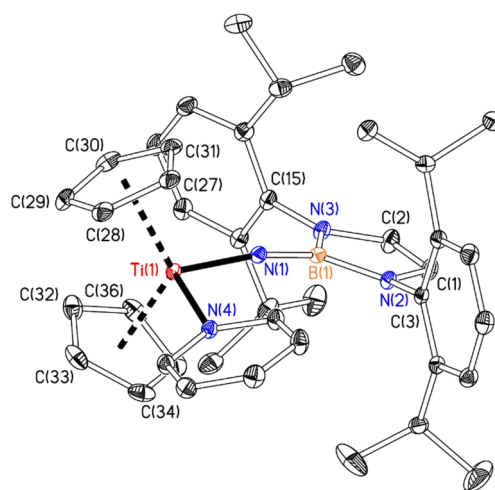
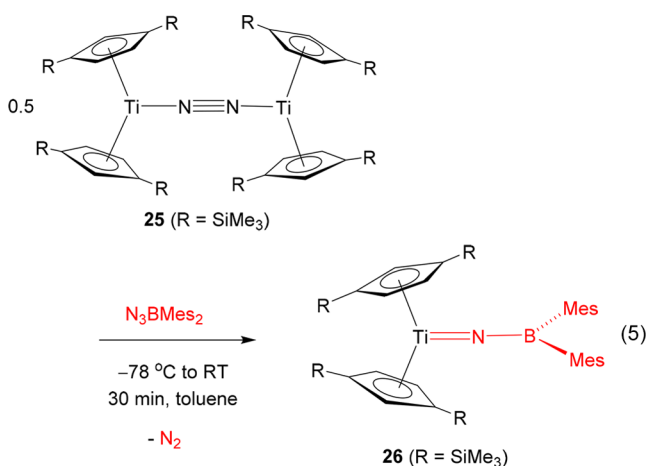


Figure 11. Displacement ellipsoid plot (20% probability) of $\text{Cp}_2\text{Ti}\{\text{NB}(\text{NAr}'\text{CH})_2\}(\text{py})$ (**23**). H atoms are omitted for clarity. Selected bond distances (Å) and angles (°): Ti(1)–N(1) 1.7549(13), Ti(1)–N(4) 2.2523(14), Ti(1)–Cp_{cent(1)} 2.22, Ti(1)–Cp_{cent(2)} 2.14, N(1)–B(1) 1.426(2), Cp_{cent(1)}–Ti(1)–N(1) 113.8, Cp_{cent(2)}–Ti(1)–N(1) 111.3, Cp_{cent(1)}–Ti(1)–N(4) 99.2, Cp_{cent(2)}–Ti(1)–N(4) 106.4, Cp_{cent(1)}–Ti(1)–Cp_{cent(2)} 125.1, N(1)–Ti(1)–N(4) 95.11(5), Ti(1)–N(1)–B(1) 159.65(12). Cp_{cent(1)} and Cp_{cent(2)} refer to the centroids for the Cp ring carbons C(27)–C(31) and C(32)–C(36), respectively.

(1.757(2) Å, Cp_{cent}–Ti–Cp_{cent} = 123.8°),^{3h} and longer than in **21** (1.723(6) Å, Cp_{cent}–Ti–Cp_{cent} = 121.3°).^{38a} These compounds also showed partial slippages of one of the Cp rings.

Bergman and Andersen have previously shown³⁹ that the base-free imide $\text{Cp}^*_2\text{Ti}(\text{NPh})$ could be prepared from $\text{Cp}^*_2\text{Ti}(\eta\text{-C}_2\text{H}_4)$ and PhN_3 , although only limited details of the solid state structure are available. Chirik subsequently found that the dinitrogen compound $(\text{Cp}^*_2\text{Ti})_2(\mu_2\text{-}\eta^1\text{-}\eta^1\text{-N}_2)$ (**25**, Cp* = 1,3-C₅H₃(SiMe₃)₂) reacts with certain azides to form $\text{Cp}^*_2\text{Ti}(\text{NR})$ (R = SiMe₃ (X-ray structure) or Xyl); Rosenthal, Schulz, and Jemmis very recently reported the X-ray structure of the arylimide $\text{Cp}^*_2\text{Ti}(\text{NAr}')$ (Ar' = 2,6-C₆H₃(Pr₂)₂), formed from $\text{Cp}^*_2\text{Ti}\{\eta\text{-C}_2(\text{SiMe}_3)_2\}$ and Ar'NCNAr'.⁴⁰

Inspired by these results and Wilkinson^{12a} and Sundermeyer's^{12b} reports of accessing certain Group 5 and 6 borylimides by reaction of lower oxidation state precursor complexes with N₃BMe₂, we carried out an analogous reaction of **25** with N₃BMe₂ in toluene at –78 °C. After warming to room temperature and workup, the base-free titanocene borylimido complex $\text{Cp}^*_2\text{Ti}(\text{NBMe}_2)$ (**26**, eq 5) was isolated as a green powder in 70% yield. The ¹H and ¹³C NMR spectra of **26** in toluene-*d*₈ solution are consistent with a C_s symmetric species having one dimesitylborylimido ligand and two Cp* groups. The ¹¹B NMR shift (44.2 ppm) is much more positive than that of **23** (18.0 ppm) or the other complexes reported above that contain NB(NAr'CH)₂ ligands (range ca. 14–18 ppm), but less than in $\text{Cp}^*_2\text{Ti}\{\text{MeC}(\text{N}^i\text{Pr})_2\}(\text{NBC}_8\text{H}_{14})$ (**2**, 52.8 ppm). These variations mainly reflect the nature of the boron substituents. The experimental ¹¹B NMR shifts for monomeric (trigonal planar) H₂NBMe₂ and H₂NB(NAr'CH)₂ are 44.5 and 22.9 ppm in C₆D₆ (DFT calculated 47.1 and 23.0 ppm). As mentioned, “H₂NBC₈H₁₄” exists as a dimer in solution and the solid state: experimental ¹¹B shift –1.7 ppm (DFT – 4.6 ppm) in C₆D₆ indicating 4-coordinate boron.⁴¹



Therefore, a direct experimental comparison with **2** cannot be made. However, the DFT calculated value of 53.8 ppm for monomeric H₂NBC₈H₁₄ is in good agreement with the trend found in the borylimides themselves.

Diffraction-quality crystals of **26** were grown from hexane at 4 °C. The solid state structure is shown in Figure 12, along with

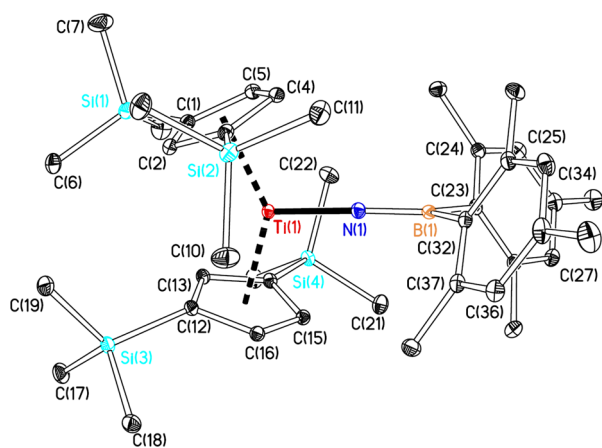


Figure 12. Displacement ellipsoid plot (20% probability) of Cp^{*}₂Ti(NBMe₂) (**26**). H atoms are omitted for clarity. Selected bond distances (Å) and angles (°): Ti(1)–N(1) 1.8069(7), Ti(1)–Cp_{cent(1)} 2.08, Ti(1)–Cp_{cent(2)} 2.08, N(1)–B(1) 1.3782(12), Cp_{cent(1)}–Ti(1)–N(1) 109.7, Cp_{cent(2)}–Ti(1)–N(1) 109.9, Cp_{cent(1)}–Ti(1)–Cp_{cent(2)} 140.5, Ti(1)–N(1)–B(1) 175.7(1). Cp_{cent(1)} and Cp_{cent(2)} refer to the centroids for Cp^{*} ring carbons C(1)–C(5) and C(12)–C(16), respectively.

selected bond distances and angles. Compound **26** is a monomeric, base-free species containing a bent Cp^{*}₂Ti moiety bonded to a NBMe₂ ligand. The mesityl rings are rotated ca. 65° out of the {N(1),B(1),C(23,32)} least-squares plane, indicating little conjugation of the aromatic rings with the Ti(1)–N(1)–B(1) linkage. The Ti(1)–N(1) distance of 1.8069(7) Å is significantly longer than the corresponding value in Cp₂Ti{NB(NAr'CH)₂}(py) (**23**), and is equal to the Ti–N_{im} distance of 1.810(1) Å in Doxsee's⁴² very delocalized {Cp₂Ti(PMe₃)₂}₂{μ-NC(Mes)C(Mes)N}, which features the longest Ti–N_{im} bond reported to date. The N(1)–B(1) distance of 1.3782(12) Å is significantly shorter than in **23** or any transition metal borylimide reported herein or previously, and is comparable to the crystallographic B–NH₂ distance of 1.375(8) Å in H₂NBMe₂ (monomeric with trigonal planar

boron).³³ The N_{im}–BMe₂ bond distances in the two previously structurally characterized examples of this type of borylimido ligand (namely, W(NMe₃)₂(NBMe₃)(PMe₃)₂ and W(NBMe₂)₂Cl₂(PMe₃)₂) were 1.39(1) and 1.43(1) Å, suggesting significantly more multiple (π-) bond character in the N_{im}–B bond of **26**.¹² There is no tendency in **26** toward ring-slippage of either Cp^{*} ring, and the Ti(1)–C distances lie in the relatively narrow range 2.364(1)–2.446(1) Å. The Ti–Cp_{cent} distances of 2.08 Å in **26** are much shorter than those in **23** (av. 2.18 ± 0.04 Å), and the Cp_{cent(1)}–Ti(1)–Cp_{cent(2)} angle of 140° is considerably larger than the value of 125.1° in **23**.

Structural comparisons can also be made with Cp^{*}₂Ti(NSiMe₃) and Cp^{*}₂Ti(NAr'), both of which are base-free like **26**, and the former has the same cyclopentadienyl ligand substituents. The Ti–N_{im} distances are 1.722(4) and 1.763(1) Å; the average Ti–Cp_{cent} distances are 2.15 and 2.12 Å; and the Cp_{cent}–Ti–Cp_{cent} angles are 128.3 and 135.3°, respectively. This seems to be consistent with the metric data for **26** and apparently implies that increasing π-accepting ability of the N_{im} substituent (anticipated to be SiMe₃ < aryl < BMe₂) drives these variations. The computational studies described below support this hypothesis.

Electronic Structure and Bonding in Bis-(cyclopentadienyl)titanium Borylimido Compounds. As mentioned, bis(cyclopentadienyl) transition metal imides are interesting particularly from a bonding point of view, being so-called “π-loaded” complexes.^{3b} These have more π-donor ligand orbitals than the metal has suitable acceptor orbitals of correct symmetry, resulting in one or more nonbonding ligand-based MOs. Early examples include tris(imido) d⁰ complexes of the type C_{3v}-M(NR)₃(L) and D_{3h}-M(NR)₃.^{3a,f,43} The new metal-locene borylimides Cp₂Ti{NB(NAr'CH)₂}(py) (**23**) and Cp^{*}₂Ti(NBMe₂) (**26**) are isolobal⁴⁴ analogues of these compounds.

At first sight **23** is a 20 valence electron compound, provided that the π-donor ligands are able to donate their maximum number of electrons (specifically 5e for Cp and 4e for the imide in the neutral electron-counting formalism⁴⁵). Compound **26** appears to be an 18 valence electron compound, but previous theoretical, spectroscopic, and structural studies of a number of Groups 4–6 complexes of the type Cp^R₂M(E)(L) (E = O or NR; L = 2- or 1-electron donor or none)^{3b,46} would suggest it should have a nonbonding, ligand-based MO. To gain a better understanding of the bonding in the new family of metallocene borylimides and metal-borylimide bonding in general we studied a small group of complexes Cp₂Ti(NR) (**2Q_R**) (Figure 13) by DFT and QTAIM methods. Calculations were also carried out on pyridine adducts Cp₂Ti(NR)(py). These gave analogous results but the analysis was less straightforward in the lower symmetry of these species.

The bonding in bent metallocenes Cp₂M(L) is usually approached by considering the interactions of the frontier molecular orbitals (FMOs) of the ligands ‘L’ with those of a bent Cp₂M moiety. The latter are well-known from previous studies.^{46a,47} For comparison we calculated the FMOs of d⁰ C_{2v}-[Cp₂Ti]²⁺ (Figure S11) at Cp_{cent}–Ti–Cp_{cent} angles of 128.5° and 135.2°, these being the angles in the optimized geometries of Cp₂Ti(NMe) (**2Q_Me**) and Cp₂Ti(NBMe₂) (**2Q_BMe₂**). [Cp₂Ti]²⁺ has three nonbonding, vacant FMOs, two of a₁ (σ) and one of b₁ (π) symmetry (in contrast to [CpTi{MeC(NMe)₂}]²⁺ (Figure S12) which has four FMOs). It is the higher energy 2a₁ FMO that interacts best with the σ-donor orbital of a ligand ‘L’ approaching along the molecular C₂

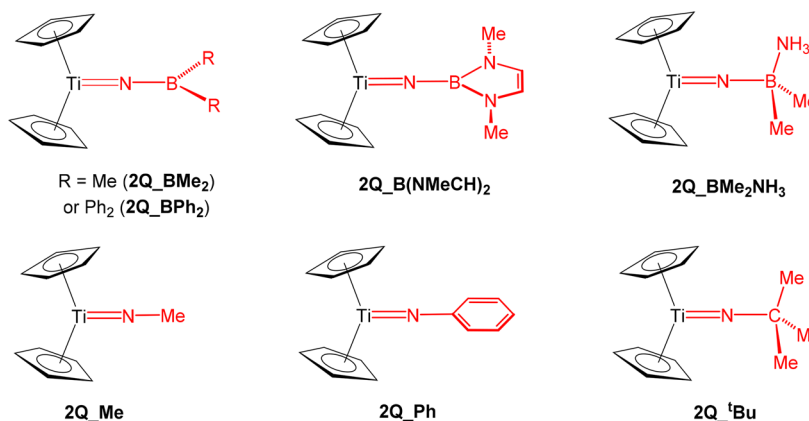


Figure 13. Model bis(cyclopentadienyl) complexes.

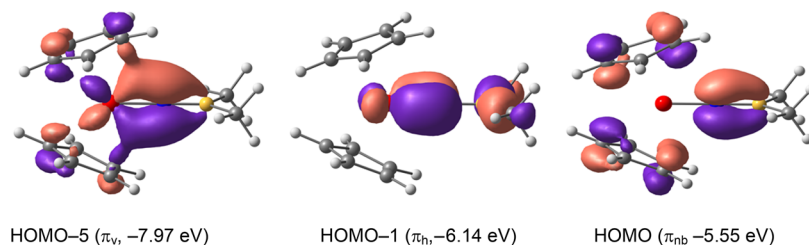


Figure 14. Selected molecular orbitals of $Cp_2Ti(NBMe_2)$ ($2Q_BMe_2$) and their energies. Isosurfaces are drawn at the 0.063 au contour level. The LUMO is shown in Figure S13 of the Supporting Information.

axis;^{46a,47} the $2b_1$ FMO lies in the horizontal mirror plane and can interact with π_h of an approaching NBR_2 or other imido ligand (according to the geometry illustrated in Figure 13). $[Cp_2Ti]^{2+}$ has no vacant π -orbital of suitable symmetry (i.e., orientation) to interact with π_v of NBR_2 . However, it is known that an out-of-plane π -interaction can take place with the LUMO+3 of d^0 Cp_2M ($2b_2$ in Figure S11), sometimes described as the “fourth frontier orbital” of a bent metallocene.^{46a} This is formally $Cp-M$ π^* antibonding and the counterpart of the $Cp-M$ π -bonding HOMO ($1b_2$ in Figure S11). Hoffmann showed that decreasing the $Cp_{cent}-Ti-Cp_{cent}$ angle of Cp_2M stabilizes $2b_2$ and destabilizes $1b_2$. Therefore, strong π_h -donation should favor a smaller angle to enhance interaction between the various FMOs involved in this interaction.⁴⁷ In addition, formal π_v -donation into $2b_2$ should also lead to longer $M-Cp_{cent}$ distances^{46a} as is found for most metallocene-imido compounds. On the other hand, it was also found that $2a_1$ and $2b_1$ are destabilized with bending,⁴⁷ and therefore good σ - and π_h -donors are predicted to favor a larger $Cp_{cent}-Ti-Cp_{cent}$ angle.

A molecular orbital analysis of $2Q_R$ found the bonding description expected from the results described above for $1Q_R$ and other studies of $Cp_2M(NR)$. Figure 14 shows the principal bonding and nonbonding π -type $Ti-N_{im}$ MOs of $2Q_BMe_2$; Figure S13 of the Supporting Information illustrates the nonbonding LUMO which is based on the $2a_1$ FMO of $[Cp_2Ti]^{2+}$. The HOMO-1 of $2Q_BMe_2$ is the $Ti-N_{im}$ π_h interaction. The corresponding π_v interaction is found in HOMO-5 which also contains significant $Cp-Ti$ bonding character. The HOMO (π_{nb}) of $2Q_BMe_2$ is wholly ligand-based and 56% Cp_2 in character, the rest being contributions from $NBMe_2$. The HOMO and HOMO-5 of $2Q_BMe_2$ arise from the three-center/four-electron-like interaction between the π_v donor of $[NBMe_2]^{2-}$ and the $1b_2$ (HOMO) and $2b_2$

(LUMO+3) FMOs of $[Cp_2Ti]^{2+}$. The electronic structures of the other $2Q_R$ compounds resemble that of $2Q_BMe_2$ with different orbital mixing from the N_{im} R-groups. There are no systematic trends in atomic contributions to π_{nb} from the Cp_2 and NR fragments due to different degrees of R-group orbital mixing, and the small changes involved.

Table 3 lists the principal geometric and QTAIM data, and bond dissociation energies for $2Q_R$. The geometric parameters agree well with their experimental counterparts considering the rather different steric factors involved. The trends in $d(Ti-N_{im})$ with R-group follow closely those in $CpTi\{MeC(NMe)_2\}(NR)$ ($1Q_R$) being shortest for R = Me or $B(NMeCH)_2$ and longest for R = BMe_2 and BPh_2 . However, whereas $d(Ti-N_{im})$ for $1Q_Me$ and $2Q_Me$ are very similar ($\Delta = 0.002$ Å), the differences (av. $\Delta = 0.03$ Å) for $1Q_BR_2$ and $2Q_BR_2$ (R = Me or Ph) are significantly larger. The $d(Ti-N_{im})$ and $d(Ti-Cp_{cent})$ distances show a strong anticorrelation ($R^2 = 0.989$), the longest $d(Ti-Cp_{cent})$ being found for the shortest $d(Ti-N_{im})$. The $Ti-N_{im}$ distances and $Cp_{cent}-Ti-Cp_{cent}$ angles directly correlate ($R^2 = 0.985$) as illustrated in Figure 15a. This is clearly due to R-group electronic effects as shown by calculations on $2Q_Me_fxd$ (Table 3 and gray diamond point in Figure 15a). Here $d(Ti-N_{im})$ was set to 1.737 Å (the same value as in $2Q_BMe_2$) and then fixed for an otherwise unconstrained geometry optimization. The resultant $d(Ti-Cp_{cent})$ and $Cp_{cent}-Ti-Cp_{cent}$ and QTAIM parameters changed very little from $2Q_Me$ itself.

In contrast, adding NH_3 to the π -accepting boron atom of $2Q_BMe_2$ to form $2Q_BMe_2NH_3$, with a non- π -accepting boron atom led to decreased values for $d(Ti-N_{im})$ and $Cp_{cent}-Ti-Cp_{cent}$ and a longer $d(Ti-Cp_{cent})$. The geometric features of the isosteric and isoelectronic $2Q_tBu$ were very similar to those of $2Q_BMe_2NH_3$, implying an important role for the π_v $Ti-N_{im}$ MO of $2Q_R$ in setting the main geometric features.

Table 3. Data for Optimized Cp₂Ti(NR) (2Q_R; R = BMe₂, BPh₂, B(NMeCH)₂, Me, Ph) and Some Related Compounds^a

compound	$d(\text{Ti}-\text{N}_{\text{im}})/d(\text{Ti}-\text{CH}_2)$ (Å)	$d(\text{Ti}-\text{Cp})$ (av., Å)	Cp-Ti-Cp (deg)	$\Delta E_{\text{Ti-N(R)}} (\text{kcal mol}^{-1})$	$\delta(\text{Ti}-\text{N}_{\text{im}})$	$\varepsilon(\text{Ti}-\text{N}_{\text{im}})/\varepsilon(\text{Ti}-\text{CH}_2)$	$\rho(\text{Ti}-\text{N}_{\text{im}})$	$\nabla^2\rho(\text{Ti}-\text{N}_{\text{im}})$	Q(NR)	Q(Cp ₂)
2Q_BMe ₂	1.737	2.082	135.2	103.3	1.496	0.363	0.193	0.673	-0.878	-0.962
2Q_BPh ₂	1.740	2.076	135.5	101.7	1.462	0.335	0.191	0.667	-0.922	-0.924
2Q_B(NMeCH) ₂	1.696	2.125	129.7	85.8	1.641	0.111	0.210	0.735	-0.829	-1.032
2Q_Me	1.677	2.140	128.5	75.2	1.692	0.111	0.209	0.846	-0.768	-1.071
2Q_Ph	1.707	2.107	131.3	75.0	1.525	0.191	0.195	0.800	-0.868	-0.981
2Q_Me _{fd}	1.737	2.128	129.3	74.6	1.627	0.140	0.182	0.775	-0.785	-1.051
Cp ₂ Ti(CH ₂)(3Q)	1.917	2.029	143.0	n.a.	n.a.	0.669	n.a.	n.a.	n.a.	-1.017
1Q_BPh ₂	1.712	n.a.	n.a.	131.2	1.545	0.193	0.204	0.701	-0.920	n.a.

^a(i) Ti-N_{im} and Ti-Cp_{cent} distances; Cp_{cent}-Ti-Cp_{cent} angle. (ii) Ti-N_{im} bond dissociation energy ($\Delta E_{\text{Ti-N(R)}}$) to relaxed S = 1 fragments. (iii) QTAIM data (atomic units) at the bond critical points: $\delta(\text{Ti}-\text{N}_{\text{im}})$, ε (electron density), $\nabla^2\rho$ (electron density Laplacian), and Q(NR) and Q(Cp₂). Not applicable: n.a.

The push-pull or buffering effect between the Ti-Cp and Ti-N_{im} interactions is also confirmed by the strong anticorrelation ($R^2 = 0.978$) between Q(Cp₂) vs Q(NR) for 2Q_R in Figure 15b (note that Q(Ti) varies little throughout the series 2Q_R, maintaining a value of ca. $+1.85 \pm 0.01$).

As a further test we calculated the geometry and QTAIM parameters of the hypothetical methyldene Cp₂Ti(CH₂) (3Q) which forms only a Ti-CH₂ σ -bond and a Ti-CH₂ π_h bond, without any additional π_v interaction. The Ti-Cp distance (2.029 Å) and Cp_{cent}-Ti-Cp_{cent} angle (143.0°) are again consistent with Ti-N_{im} bond π_v effects, rather than π_h or σ effects, being the most important in setting the geometries of Cp₂Ti(NR) and their real counterparts. Although a base-free titanium alkylidene analogous to 3Q has not been isolated and crystallographically characterized, we note that the Cp_{cent}-Ti-Cp_{cent} angle of 143.2° in the d² compound Cp₂W(CHPh)⁴⁸ is very similar to than in 3Q while the corresponding angle in d² Cp₂Mo(N^tBu)^{46c} is 127.9°, very close to the 128.5° value calculated for 2Q_Me and 2Q_1Bu.

The trends in the principal QTAIM parameters and bond dissociation energy with N_{im} R-group type (Table 3) for 2Q_R parallel those found for 1Q_R, with the Figure 15c,d showing a strong correlation between the $\Delta E_{\text{Ti-N(R)}}$ values for 2Q_R and those for 1Q_R ($R^2 = 0.993$), and an anticorrelation between $\Delta E_{\text{Ti-N(R)}}$ and $\nabla^2\rho$ ($R^2 = 0.925$). These relationships and the other QTAIM data for 2Q_R show that the underlying electronic factors controlling the bond energies in the metallocene systems are the same as in the cyclopentadienylamidates 1Q_R. Also as in the 1Q_R series, the Ti-N_{im} bond lengths in 2Q_R are dominated by Ti-N_{im} π_v bonding effects. The latter are further amplified by the π -loaded nature of these metallocene derivatives, giving disproportionately longer Ti-N_{im} bonds, smaller $\delta(\text{Ti}-\text{N}_{\text{im}})$ indices, and larger ε values for the most π -accepting BR₂ (R = Me, Ph).

CONCLUSIONS

In this contribution we have developed synthetic entry points to two classes of borylimido compounds, namely, those based on N,N-substituted boryl substituents ((L)Ti{NB-(NAr'CH)₂}) and one with a diarylboryl substituent (i.e., Cp''₂Ti(NBMe₂) (26)). For the former type it was possible to use either a double-deprotonation strategy starting from Ti(NMe₂)₂Cl₂ or endergonic borylamine-*tert*-butylimide exchange, provided that the latter was driven in favor of the product. Neither of these protocols is thermodynamically feasible for dialkyl- or diarylborylamines. However, oxidative methods seem to be suitable for appropriate precursors, for example, reaction of (Cp''₂Ti)₂($\mu_2\eta^1\eta^1\text{-N}_2$) with N₃BMe₂ to form 26. The three synthetic methods gave access to sandwich or half-sandwich borylimido compounds, as well as the useful synthons Ti{NB(NAr'CH)₂}Cl₂(NHMe₂)₂ and Ti{NB(NAr'CH)₂}Cl₂(py)₃.

With specific regard to the protonolysis methods, the main limitation is the strong H-N bonds of the borylamines compared to the bond strengths of the product imide. Other routes for imido groups from amines are, in principle, available: for example, alkane elimination from alkyl-amide precursors of the type (L)M{N(H)BR₂}R' as previously demonstrated for Group 4 organoimido compounds.^{1b,f,15,49} An exploration of these routes was beyond the scope of our current study.

The QTAIM and NBO studies showed that two key descriptors of the metal-nitrogen multiple bond in imido and hydrazido compounds, namely, the bond distance and the

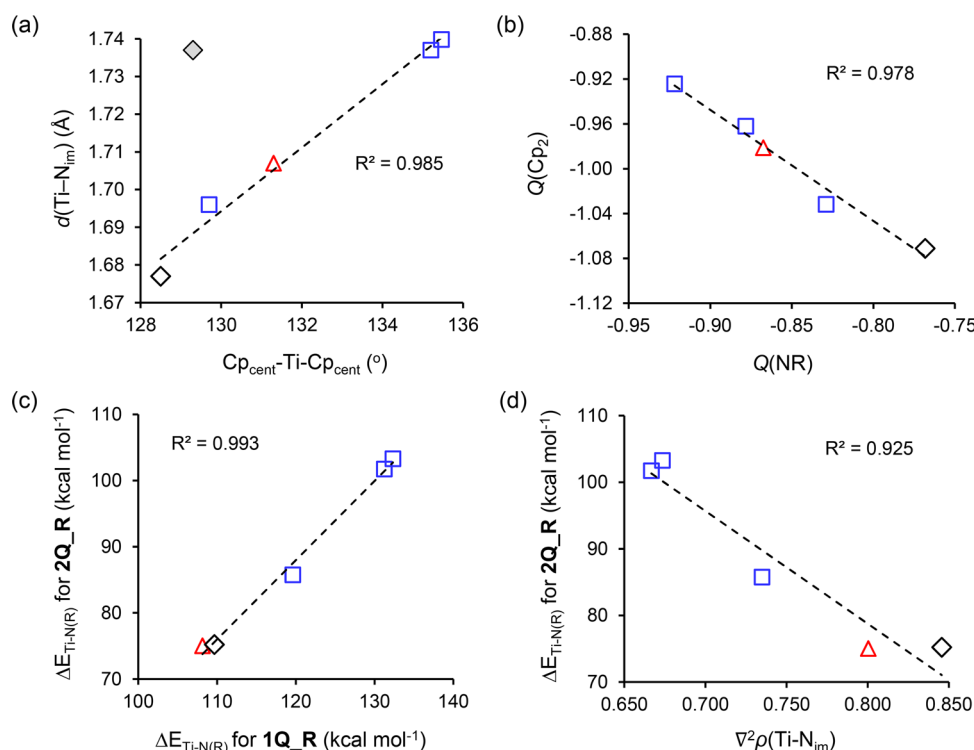


Figure 15. (a) Plot of $d(\text{Ti}-\text{N}_{\text{im}})$ vs. $\text{Cp}_{\text{cent}}-\text{Ti}-\text{Cp}_{\text{cent}}$ for **2Q_R**; the filled black diamond (not included in the linear regression) is for **2Q_Me_fixd** ($\text{Ti}-\text{N}_{\text{im}} = 1.737$ Å). (b) Plot of $Q(\text{Cp}_2)$ vs $Q(\text{NR})$ for **2Q_R**. Plots of $\Delta E_{\text{Ti-N(R)}}$ for $\text{Cp}_2\text{Ti}(\text{NR})$ (**2Q_R**) vs (c) $\Delta E_{\text{Ti-N(R)}}$ for $\text{CpTi}\{\text{MeC}(\text{NMe})_2\}(\text{NR})$ (**1Q_R**) and (d) $\nabla^2\rho$ (electron density Laplacian) for **2Q_R**. Key for all plots: blue squares, R = BMe₂, BPh₂, B(NMeCH)₂; open black diamond, R = Me; red triangle, R = Ph.

bond dissociation energy, are separable and arise from distinct electronic factors. The variation in the Ti–N_{im} bond distance is found to be dominated by π interactions with the substituent at the N_{im} atom, while variation in the bond dissociation energy is found to arise primarily from the underlying σ -donor and π -donor ability of the NR fragment, which in turn relates to the electronegativity of the R substituent. It is the latter effect which controls the favorability or otherwise of imide-amine exchange reactions, and the difficulties in forming borylimides through this methodology are found to arise from the high N–H bond strengths in the corresponding borylamines, even though the Ti–N_{im} bonds of borylimides are the strongest of all the types of titanium imido compound (L)₂Ti(NR) (R = hydrocarbyl or NR').

EXPERIMENTAL SECTION

Representative syntheses and characterizing data (noncyclopentadienyl, half-sandwich and metallocene) are given below. General experimental procedures, details of starting materials, and syntheses and characterization of all the other new compounds are given in the Supporting Information.

Ti[NB(NAr'CH)₂]Cl₂(NHMe)₂ (8). To a solution of Ti(NMe₂)₂Cl₂ (1.36 g, 6.58 mmol) in toluene (10 mL) was slowly added a solution of H₂NB(NAr'CH)₂ (6, 2.52 g, 6.25 mmol) in toluene (10 mL), at –78 °C. The mixture was allowed to warm to room temperature, upon which it became a red/brown slurry. After stirring for 30 min, all solids had dissolved, leaving a deep red solution, which was stirred at room temperature for a further 2.5 h. The volatiles were then removed under reduced pressure to leave a red-brown, waxy solid. The product was triturated in hexane, yielding **8** as an orange-brown powder. Yield: 3.01 g (79%). Diffraction-quality crystals were grown from a saturated hexane solution at room temperature. ¹H NMR (C₆D₆, 400.1 MHz): δ 7.13 (6 H, overlapping 2 × m, m- and p-C₆H₃Pr₂), 5.73 (2 H, s, NCH), 3.53 (4 H, sept., ³J = 6.9 Hz, CHMeMe), 2.67 (2 H, sept., ³J =

6.1 Hz, NHMe₂), 1.92 (12 H, d, ³J = 6.1 Hz, NHMe₂), 1.56 (12 H, d, ³J = 6.9 Hz, CHMeMe), 1.24 (12 H, d, ³J = 6.9 Hz, CHMeMe) ppm. ¹³C{¹H} NMR (C₆D₆, 100.6 MHz): δ 146.8 (i-C₆H₃Pr₂), 140.2 (o-C₆H₃Pr₂), 127.2 (p-C₆H₃Pr₂), 123.3 (m-C₆H₃Pr₂), 115.5 (NCH), 40.0 (NHMe₂), 28.4 (CHMeMe), 24.2 (CHMeMe), 24.0 (CHMeMe) ppm. ¹¹B{¹H} NMR (C₆D₆, 128.4 MHz): δ 14.2 ppm. IR (NaCl plates, Nujol mull, cm⁻¹): 3289 (w, nonbridging N–H), 3277 (w, hydrogen bonded N–H), 1586 (m), 1260 (w), 1180 (w), 1076 (w), 1025 (m), 983 (m), 890 (m), 798 (m), 686 (w), 652 (m). IR (NaCl cell, CH₂Cl₂, $\nu(\text{N}-\text{H})$, cm⁻¹): 3288. Anal. found (calcd. for C₃₀H₅₀BCl₂N₅Ti): C, 58.95 (59.04); H, 8.18 (8.26); N, 11.37 (11.47)%.

Cp*Ti[NB(NAr'CH)₂]Cl(py) (15). To a Schlenk flask were added Cp*Ti(N^tBu)Cl(py) (**14**, 2.00 g, 5.42 mmol) and H₂NB(NAr'CH)₂ (**6**, 1.97 g, 4.88 mmol). The two solids were heated with stirring to 140 °C, at which temperature they melted to form a dark brown oil. Repeated, brief exposures to a dynamic vacuum resulted in bubbling of the oil as H₂N^tBu was released; the cessation of bubbling and no further diminishment of the vacuum (as measured by a Pirani gauge) indicated reaction completion. The oil was allowed to cool to room temperature, forming a deep red glassy solid, which was triturated in hexane (10 mL) to yield **15** as a red powder, before washing with further hexane (2 × 10 mL) and drying *in vacuo*. Yield: 2.02 g (59%). Diffraction-quality crystals were grown from a saturated benzene/hexane solution at room temperature. ¹H NMR (C₆D₆, 400.1 MHz): δ 7.88 (2 H, d, ³J = 4.7 Hz, 2,6-py), 7.25 (2 H, dd, ³J = 7.8 Hz, ⁴J = 1.5 Hz, m-C₆H₃Pr₂ closest to py), 7.17–7.12 (2 H, m overlapping with residual protio solvent resonance, p-C₆H₃Pr₂), 7.00 (2 H, dd, ³J = 7.8 Hz, ⁴J = 1.5 Hz, m-C₆H₃Pr₂ closest to Cl), 6.65 (1 H, t, ³J = 7.8 Hz, 4-py), 6.22 (2 H, m, 3,5-py), 5.87 (2 H, s, NCH), 3.92 (2 H, sept., ³J = 6.9 Hz, CHMeMe closest to py), 3.67 (2 H, sept., ³J = 6.9 Hz, CHMeMe closest to Cl), 1.71 (15 H, s, C₅Me₅), 1.61 (6 H, d, ³J = 6.8 Hz, CHMeMe closest to py), 1.31 (12 H, app. t, app. ³J = 7.3 Hz, overlapping CHMeMe closest to py and CHMeMe closest to Cl), 1.26 (6 H, d, ³J = 6.8 Hz, CHMeMe closest to Cl) ppm. ¹³C{¹H} NMR

(C₆D₆, 100.6 MHz): δ 150.4 (2,6-py), 147.3 (*o*-C₆H₃Pr₂ closest to Cl), 147.0 (*o*-C₆H₃Pr₂ closest to py), 141.9 (*i*-C₆H₃Pr₂), 126.9 (*p*-C₆H₃Pr₂), 123.8 (3,5-py), 123.8 (*m*-C₆H₃Pr₂ closest to Cl), 123.1 (*m*-C₆H₃Pr₂ closest to py), 121.8 (C₅Me₅), 116.9 (NCH), 29.0 (CHMeMe closest to py), 28.4 (CHMeMe closest to Cl), 26.0 (CHMeMe closest to Cl), 24.9 (CHMeMe closest to py), 24.2 (CHMeMe closest to Cl), 23.6 (CHMeMe closest to py), 12.0 (C₅Me₅) ppm. ¹¹B{¹H} NMR (C₆D₆, 128.4 MHz): δ 15.5 ppm. IR (NaCl plates, Nujol mull, cm⁻¹): 3583 (w), 3064 (m), 2724 (m), 1936 (w), 1868 (w), 1801 (w), 1663 (m), 1606 (s), 1585 (w), 1328 (m), 1308 (w), 1275 (m), 1215 (m), 1178 (w), 1154 (m), 1114 (m), 1070 (m), 1046 (m), 1017 (w), 1009 (w), 894 (m), 883 (w), 803 (m), 763 (m), 755 (m), 721 (w), 681 (w), 651 (s). EI-MS: *m/z* = 698 [M]⁺ (1%). Anal. found (calcd. for C₄₁H₅₆BClN₄Ti): C, 70.35 (70.45); H, 7.95 (8.07); N, 7.95 (8.01)%.

Cp₂Ti(NB(NAr'CH)₂)(py) (23). To a Schlenk flask containing Ti{NB(NAr'CH)₂Cl₂}(py)₃ (9, 0.500 g, 0.660 mmol) and NaCp (0.122 g, 1.39 mmol) was added toluene (10 mL) at -78 °C. The mixture was allowed to warm to room temperature, and then stirred for 3 h, after which it had become a deep brown suspension. The volatiles were removed under reduced pressure, and the product extracted into pentane (4 × 10 mL). The combined extracts were evaporated to dryness, giving **23** as an orange powder. Yield: 0.253 g (58%). Diffraction-quality crystals were grown from a concentrated pentane solution at 5 °C. ¹H NMR (C₆D₆, 400.1 MHz): δ 7.96 (2 H, d, ³J = 4.9 Hz, 2,6-py), 7.31–7.25 (6 H, overlapping 2 × m, *m*- and *p*-C₆H₃Pr₂), 6.71 (1 H, t, ³J = 7.7 Hz, 4-py), 6.23 (2 H, m, 3,5-py), 5.94 (2 H, s, NCH), 5.69 (10 H, s, C₅H₅), 3.74 (4 H, sept., ³J = 6.9 Hz, CHMeMe), 1.49 (12 H, d, ³J = 6.9 Hz, CHMeMe), 1.30 (12 H, d, ³J = 6.9 Hz, CHMeMe) ppm. ¹³C{¹H} NMR (C₆D₆, 100.6 MHz): δ 155.1 (2,6-py), 147.5 (*o*-C₆H₃Pr₂), 142.2 (*i*-C₆H₃Pr₂), 136.4 (4-py), 127.0 (*m*-C₆H₃Pr₂), 123.7 (*p*-C₆H₃Pr₂), 123.6 (3,5-py), 117.2 (NCH), 111.4 (C₅H₅), 28.9 (CHMeMe), 25.7 (CHMeMe), 23.6 (CHMeMe) ppm. ¹¹B{¹H} NMR (C₆D₆, 128.4 MHz): δ 18.0 ppm. IR (NaCl plates, Nujol mull, cm⁻¹): 1602 (m), 1583 (w), 1543 (m), 1403 (w), 1215 (m), 1178 (w), 1068 (m), 1023 (m), 936 (w), 883 (w), 863 (s), 763 (w), 699 (m), 668 (m), 653 (w). EI-MS: *m/z* = 580 [M - py]⁺ (4%). Anal. found (calcd. for C₄₁H₅₁BN₄Ti): C, 74.61 (74.78); H, 7.96 (7.81); N, 8.64 (8.51)%.

■ ASSOCIATED CONTENT

■ Supporting Information

The Supporting Information is available free of charge on the ACS Publications website at DOI: 10.1021/acs.inorgchem.7b01831.

Details of starting materials. Remaining details of the synthesis and characterizing data for new compounds. Computational details and total SCF and other energies for DFT computed structures (PDF)

Computed Cartesian coordinates of all of the molecules reported in this study. The file may be opened as a text file to read the coordinates, or opened directly by a molecular modeling program such as Mercury (version 3.3 or later, <http://www.ccdc.cam.ac.uk/pages/Home.aspx>) for visualization and analysis (XYZ)

Accession Codes

CCDC 1555531–1555541 contain the supplementary crystallographic data for this paper. These data can be obtained free of charge via www.ccdc.cam.ac.uk/data_request/cif, or by emailing data_request@ccdc.cam.ac.uk, or by contacting The Cambridge Crystallographic Data Centre, 12 Union Road, Cambridge CB2 1EZ, UK; fax: +44 1223 336033.

■ AUTHOR INFORMATION

Corresponding Authors

*(E.C.) E-mail: eric.clot@umontpellier.fr.

*(P.M.) E-mail: philip.mountford@chem.ox.ac.uk.

ORCID

Eric Clot: 0000-0001-8332-5545

Philip Mountford: 0000-0001-9869-9902

Notes

The authors declare no competing financial interest.

■ ACKNOWLEDGMENTS

This work was funded by the EPSRC (Grant Reference EP/L505031/1), the University of Oxford Clarendon Fund and the University of Oxford SCG Innovation Fund. We thank the University of Oxford's Advanced Research Computing facility for access to supercomputer and other resources. The authors declare no competing financial interests.

■ REFERENCES

- (1) (a) Wigley, D. E. Organoimido complexes of the transition metals. *Prog. Inorg. Chem.* **1994**, 42, 239–482. (b) Duncan, A. P.; Bergman, R. G. Selective Transformations of Organic Compounds by Imidozirconocene Complexes. *Chem. Rev.* **2002**, 2, 431–445. (c) Mountford, P. New titanium imido chemistry. *Chem. Commun.* **1997**, 2127–2134. (d) Gade, L. H.; Mountford, P. New transition metal imido chemistry with diamido-donor ligands. *Coord. Chem. Rev.* **2001**, 216–217, 65–97. (e) Hazari, N.; Mountford, P. Reactions and applications of titanium imido compounds. *Acc. Chem. Res.* **2005**, 38, 839–849. (f) Fout, A. R.; Kilgore, U. J.; Mindiola, D. J. The Progression of Synthetic Strategies to Assemble Titanium Complexes Bearing the Terminal Imide Group. *Chem. - Eur. J.* **2007**, 13, 9428–9440.
- (2) (a) Walsh, P. J.; Hollander, F. J.; Bergman, R. G. Generation, alkyne cycloaddition, C-H activation, N-H activation and dative ligand trapping reactions of the first monomeric imidozirconocene complexes. *J. Am. Chem. Soc.* **1988**, 110, 8729–8731. (b) Hill, J. E.; Profflet, R. D.; Fanwick, P. E.; Rothwell, I. P. Synthesis, structure and reactivity of aryloxo(imido)titanium complexes. *Angew. Chem., Int. Ed. Engl.* **1990**, 29, 664–665. (c) Roesky, H. W.; Voelker, H.; Witt, M.; Noltemeyer, M. Synthesis and Structure of Ph₂P(S)N = TiCl₂3py, the first imidotitanium complex. *Angew. Chem., Int. Ed. Engl.* **1990**, 29, 669–670. (d) Cummins, C. C.; Baxter, S. M.; Wolczanski, P. T. Methane and benzene C-H activation via transient (t-Bu₃SiNH)₂Zr(=NSi^tBu₃). *J. Am. Chem. Soc.* **1988**, 110, 8731–8733.
- (3) (a) Cundari, T. R. Transition metal imido complexes. *J. Am. Chem. Soc.* **1992**, 114, 7879–7888. (b) Lin, Z.; Hall, M. B. A group theoretical analysis on transition metal complexes with metal-ligand multiple bonds. *Coord. Chem. Rev.* **1993**, 123, 149–167. (c) Mountford, P.; Swallow, D. A direct relationship between E=T-L bond angle and E=Ti bond length can exist in [Ti(E)L₄] complexes (E = organoimido or oxo). *J. Chem. Soc., Chem. Commun.* **1995**, 2357–2359. (d) Kaltsayannis, N.; Mountford, P. Theoretical studies of the geometric and electronic structures of pseudo-octahedral d⁰ imido compounds of titanium: the *trans* influence in *mer*-[Ti(NR)-Cl₂(NH₃)₃] (R = Bu^t, C₆H₅ or C₆H₄NO₂-4). *J. Chem. Soc., Dalton Trans.* **1999**, 781–789. (e) Cundari, T. R. Computational Studies of Transition Metal - Main Group Multiple Bonding. *Chem. Rev.* **2000**, 100, 807–818. (f) Schwarz, A. D.; Nielson, A. J.; Kaltsayannis, N.; Mountford, P. The first group 4 metal bis(imido) and tris(imido) complexes. *Chem. Sci.* **2012**, 3, 819–824. (g) Blake, A. J.; Dunn, S. C.; Green, J. C.; Jones, N. M.; Moody, A. G.; Mountford, P.; Dunn, S. C. Synthesis and Molecular and Electronic Structure of Monomeric [Ti(η-C₈H₈)(N^tBu)]. *Chem. Commun.* **1998**, 1235–1236. (h) Selby, J. D.; Feliz, M.; Schwarz, A. D.; Clot, E.; Mountford, P. New Sandwich and Half-Sandwich Titanium Hydrazido Compounds. *Organometallics* **2011**, 30, 2295–2307. (i) Boyd, C. L.; Clot, E.; Guiducci, A. E.; Mountford, P. Pendant arm functionalised benzamidinate titanium imido compounds: experimental and computational studies of their reactions with CO₂. *Organometallics* **2005**, 24, 2347–2367.

- (4) (a) Mindiola, D. J. Early Transition-Metal Hydrazido Complexes: Masked Metallanitrenes from N–N Bond Scission. *Angew. Chem., Int. Ed.* **2008**, *47*, 1557–1559. (b) Walsh, P. J.; Carney, M. J.; Bergman, R. G. Generation, Dative Ligand trapping and N–N bond cleavage reactions of the first monomeric η^1 -hydrazido zirconocene complex, $\text{Cp}_2\text{Zr}=\text{NNPh}_2$. A zirconium-mediated synthesis of indoles. *J. Am. Chem. Soc.* **1991**, *113*, 6343–6345. (c) Cao, C.; Shi, Y.; Odom, A. L. Intermolecular Alkyne Hydroaminations Involving 1,1-Disubstituted Hydrazines. *Org. Lett.* **2002**, *4*, 2853–2856. (d) Li, Y.; Shi, Y.; Odom, A. L. Titanium Hydrazido and Imido Complexes: Synthesis, Structure, Reactivity, and Relevance to Alkyne Hydroamination. *J. Am. Chem. Soc.* **2004**, *126*, 1794–1803. (e) Banerjee, S.; Odom, A. L. Synthesis and Structure of a Titanium Hydrazido(2-) Complex. *Organometallics* **2006**, *25*, 3099–3101. (f) Dissanayake, A. A.; Odom, A. L. Single-step synthesis of pyrazoles using titanium catalysis. *Chem. Commun.* **2012**, *48*, 440–442. (g) Herrmann, H.; Lloret Fillol, J. L.; Wadepohl, H.; Gade, L. H. A Zirconium Hydrazide as a Synthone for a Metallanitrene Equivalent: Atom-by-Atom Assembly of $[\text{EN}_2]_2$ Units (E = S, Se) by Chalcogen-Atom Transfer in the Coordination Sphere of a Transition Metal. *Angew. Chem., Int. Ed.* **2007**, *46*, 8426–8430. (h) Gehrman, T.; Lloret Fillol, J. L.; Wadepohl, H.; Gade, L. H. Assembly of an R_3N_3 Chain by Cycloaddition of a Hydrazinediide and an Azide at Zirconium and its Thermal Fragmentation. *Angew. Chem., Int. Ed.* **2009**, *48*, 2152–2156. (i) Gehrman, T.; Kruck, M.; Wadepohl, H.; Gade, L. H. Stitching together SN_x units in the coordination sphere of zirconium: assembly of a tris(imido)sulfite and a hydrazidobis(imido)-sulfite. *Chem. Commun.* **2012**, *48*, 2397–2399. (j) Gehrman, T.; Scholl, S. A.; Fillol, J. L.; Wadepohl, H.; Gade, L. H. Alternative Reaction Pathways in Domino Reactions of Hydrazinediidozirconium Complexes with Alkynes. *Chem. - Eur. J.* **2012**, *18*, 3925–3942. (k) Blake, A. J.; McInnes, J. M.; Mountford, P.; Nikonov, G. I.; Swallow, D.; Watkin, D. J. Cycloaddition Reactions of Titanium and Zirconium Imido, Oxo and Hydrazido Complexes Supported by Tetraaza Macrocyclic Ligands. *J. Chem. Soc., Dalton Trans.* **1999**, 379–392. (l) Selby, J. D.; Manley, C. D.; Feliz, M.; Schwarz, A. D.; Clot, E.; Mountford, P. New ligand platforms for developing the chemistry of the $\text{Ti}=\text{N}-\text{NR}_2$ functional group and insertion of alkynes into the N–N bond of a $\text{Ti}=\text{N}-\text{NPh}_2$ ligand. *Chem. Commun.* **2007**, 4937–4939. (m) Schofield, A. D.; Nova, A.; Selby, J. D.; Manley, C. D.; Schwarz, A. D.; Clot, E.; Mountford, P. $\text{M}=\text{N}_\alpha$ cycloaddition and $\text{N}_\alpha-\text{N}_\beta$ insertion in the reactions of titanium hydrazido compounds with alkynes: a combined experimental and computational study. *J. Am. Chem. Soc.* **2010**, *132*, 10484–10497. (n) Tiong, P. J.; Schofield, A. D.; Selby, J. D.; Nova, A.; Clot, E.; Mountford, P. Single and double substrate insertion into the $\text{Ti}=\text{N}_\alpha$ bonds of terminal titanium hydrazides. *Chem. Commun.* **2010**, *46*, 85–87. (o) Schofield, A. D.; Nova, A.; Selby, J. D.; Schwarz, A. D.; Clot, E.; Mountford, P. Reaction site diversity in the reactions of titanium hydrazides with organic nitriles, isonitriles and isocyanates: $\text{Ti}=\text{N}$ cycloaddition, $\text{Ti}=\text{N}$ insertion and N–N bond cleavage. *Chem. - Eur. J.* **2011**, *17*, 265–285. (p) Tiong, P. J.; Nova, A.; Schwarz, A. D.; Selby, J. D.; Clot, E.; Mountford, P. Site selectivity and reversibility in the reactions of titanium hydrazides with $\text{Si}-\text{H}$, $\text{Si}-\text{X}$, $\text{C}-\text{X}$ and H^+ reagents: $\text{Ti}-\text{N}_\alpha$ 1,2-silane addition, N_β alkylation, N_α protonation and σ -bond metathesis. *Dalton Trans.* **2012**, *41*, 2277–2288. (q) Stevenson, L. C.; Mellino, S.; Clot, E.; Mountford, P. Reactions of Titanium Hydrazides with Silanes and Boranes: N–N Bond Cleavage and N Atom Functionalization. *J. Am. Chem. Soc.* **2015**, *137*, 10140–10143. (r) Tiong, P. J.; Groom, L. R.; Clot, E.; Mountford, P. Synthesis, Bonding and Reactivity of a Terminal Titanium Alkylidene Hydrazido Compound. *Chem. - Eur. J.* **2013**, *19*, 4198–4216. (5) Wiberg, N.; Haring, H.-W.; Huttner, G.; Friedrich, P. [Bis(trimethylsilyl)isodiazene](cyclopentadienyl)metall-Komplexe: Synthese und Struktur. *Chem. Ber.* **1978**, *111*, 2708–2715. (6) (a) Schwarz, A. D.; Nova, A.; Clot, E.; Mountford, P. Titanium alkoxyimido ($\text{Ti}=\text{N}-\text{OR}$) complexes: reductive N–O bond cleavage at the boundary between hydrazide and peroxide ligands. *Chem. Commun.* **2011**, *47*, 4926–4928. (b) Schwarz, A. D.; Nova, A.; Clot, E.; Mountford, P. Titanium *tert*-Butoxyimido Compounds. *Inorg. Chem.* **2011**, *50*, 12155–12171. (c) Groom, L. R.; Russell, A. F.; Schwarz, A. D.; Mountford, P. Reactions of a Cyclopentadienyl–Amidinate Titanium Benzimidamido Complex. *Organometallics* **2014**, *33*, 1002–1009. (d) Groom, L. R.; Schwarz, A. D.; Nova, A.; Clot, E.; Mountford, P. Synthesis and reactions of a cyclopentadienyl-amidinate titanium *tert*-butoxyimido compound. *Organometallics* **2013**, *32*, 7520–7539. (7) Weinhold, F.; Landis, C. R. *Valency and Bonding: A Natural Bond Orbital Donor-Acceptor Perspective*; Cambridge University Press: Cambridge, 2005. (8) (a) Selby, J. D.; Manley, C. D.; Schwarz, A. D.; Clot, E.; Mountford, P. Titanium hydrazides supported by diamide-amine and related ligands: a combined experimental and DFT study. *Organometallics* **2008**, *27*, 6479–6494. (b) Tiong, P. J.; Nova, A.; Groom, L. R.; Schwarz, A. D.; Selby, J. D.; Schofield, A. D.; Clot, E.; Mountford, P. Reactions of cyclopentadienyl-amidinate titanium hydrazides with CO_2 , CS_2 and isocyanates: $\text{Ti}=\text{N}$ cycloaddition, cycloaddition insertion and cycloaddition- NNR_2 group transfer reactions. *Organometallics* **2011**, *30*, 1182–1201. (9) (a) Protchenko, A. V.; Saleh, L. M. A.; Vidovic, D.; Dange, D.; Jones, C.; Mountford, P.; Aldridge, S. Contrasting reactivity of anionic boron- and gallium-containing NHC analogues: E–C vs. E–M bond formation (E = B, Ga). *Chem. Commun.* **2010**, *46*, 8546–8548. (b) Saleh, L. M. A.; Hassomal Birj Kumar, K.; Protchenko, A. V.; Schwarz, A. D.; Aldridge, S.; Jones, C.; Kaltsoyannis, N.; Mountford, P. Group 3 and Lanthanide Boryl Compounds: Syntheses, Structures, and Bonding Analyses of Sc-B, Y-B, and Lu-B σ -Coordinated NHC Analogues. *J. Am. Chem. Soc.* **2011**, *133*, 3836–3839. (10) Thompson, R.; Chen, C.-H.; Pink, M.; Wu, G.; Mindiola, D. J. A Nitrido Salt Reagent of Titanium. *J. Am. Chem. Soc.* **2014**, *136*, 8197–8200. (11) Grant, L. N.; Pinter, B.; Kurogi, T.; Carroll, M. E.; Wu, G.; Manor, B. C.; Carroll, P. J.; Mindiola, D. J. Molecular titanium nitrides: nucleophiles unleashed. *Chem. Sci.* **2017**, *8*, 1209–1224. (12) (a) Danopoulos, A. A.; Redshaw, C.; Vaniche, A.; Wilkinson, G.; Hussain-Bates, B.; Hursthouse, M. B. Organonitride complexes of tungsten- X-ray crystal structures of $\text{W}(\text{NC}_6\text{H}_{11})\text{Cl}_2(\text{PMe}_3)_3$, $[\text{W}(\text{NC}_6\text{H}_{11})\text{Cl}_2(\text{PMe}_3)_3]_3\text{O}_3\text{SCF}_3$, $[\text{W}(\text{NC}_6\text{H}_{11})\text{Cl}(\text{PMe}_3)_4]\text{BPh}_4$, $[\text{W}(\text{NSi}(\text{O}-\text{MeC}_6\text{H}_4)_3)\text{Cl}_2(\text{PMe}_3)_3]$, $[\text{W}(\text{NB}(\text{Mes}_2))_2\text{Cl}_2(\text{PMe}_3)_2]$, $\text{W}(\text{NPh})\text{Cl}[\text{O}_2\text{C}_2(\text{CF}_3)_4]_2\text{Li}$ and $\text{WCl}_4(\text{PMe}_2\text{Ph})_3$. *Polyhedron* **1993**, *12*, 1061–1071. (b) Weber, K.; Korn, K.; Schorm, A.; Kipke, J.; Lemke, M.; Khvorost, A.; Harms, K.; Sundermeyer, J. Recent Advances in the Synthesis of N-Heteroatom Substituted Imido Complexes Containing a Nitrido Bridge $[\text{M}=\text{N}-\text{E}]$ (M = Group 4, 5 and 6 Metal, E = B, Si, Ge, P, S). *Z. Anorg. Allg. Chem.* **2003**, *629*, 744–754. (13) Fryzuk, M. D.; MacKay, B. A.; Johnson, S. A.; Patrick, B. O. Hydroboration of Coordinated Dinitrogen: A New Reaction for the N_2 Ligand that Results in Its Functionalization and Cleavage. *Angew. Chem., Int. Ed.* **2002**, *41*, 3709–3712. (14) Hadlington, T. J.; Abdalla, J. A. B.; Tirfoin, R.; Aldridge, S.; Jones, C. Stabilization of a two-coordinate, acyclic diaminosilylene (ADASi): completion of the series of isolable diaminotetraylenes, $\text{E}-(\text{NR}_2)_2$ (E = group 14 element). *Chem. Commun.* **2016**, *52*, 1717–1720. (15) Clough, B. A.; Mellino, S.; Clot, E.; Mountford, P. New scandium borylimido chemistry: synthesis, bonding and reactivity. *J. Am. Chem. Soc.* **2017**, *139*, 11165–11183. (16) (a) Bettinger, H. F. Phenylborylene: Direct spectroscopic characterization in inert gas matrices. *J. Am. Chem. Soc.* **2006**, *128*, 2534–2535. (b) Bettinger, H. F.; Bornemann, H. Donor stabilized borylnitrene: A highly reactive BN analogue of vinylidene. *J. Am. Chem. Soc.* **2006**, *128*, 11128–11134. (c) Bettinger, H. F. BN-analogues of vinylidene transition metal complexes: The borylnitrene isomer. *Inorg. Chem.* **2007**, *46*, 5188–5195. (d) Bettinger, H. F.; Filthaus, M.; Bornemann, H.; Oppel, I. M. Metal-free conversion of methane and cycloalkanes to amines and amides by employing a borylnitrene. *Angew. Chem., Int. Ed.* **2008**, *47*, 4744–4747. (e) Bettinger, H. F.; Filthaus, M.; Neuhaus, P. Insertion into

- dihydrogen employing the nitrogen centre of a borylnitrene. *Chem. Commun.* **2009**, 2186–2188. (f) Filthaus, M.; Schwertmann, L.; Neuhaus, P.; Seidel, R. W.; Oppel, I. M.; Bettinger, H. F. C–H bond amination by photochemically generated transient borylnitrenes at room temperature: A combined experimental and theoretical investigation of the insertion mechanism and influence of substituents. *Organometallics* **2012**, *31*, 3894–3903. (g) Müller, M.; Maichle-Mössmer, C.; Bettinger, H. F. C–H functionalization of tetramethylsilane employing a borylnitrene. *Chem. Commun.* **2013**, 49, 11773–11775.
- (17) (a) Blake, A. J.; Collier, P. E.; Dunn, S. C.; Li, W.-S.; Mountford, P.; Shishkin, O. V. Synthesis and imido-group exchange reactions of *tert*-butylimidotitanium complexes. *J. Chem. Soc., Dalton Trans.* **1997**, 1549–1558. (b) Dunn, S. C.; Batsanov, A. S.; Mountford, P. A general route to Ti imido complexes: structure of $[(\text{Me}_8\text{ta})\text{Ti}(\text{NBU}^t)]$. *J. Chem. Soc., Chem. Commun.* **1994**, 2007–2008. (c) Adams, N.; Bigmore, H. R.; Blundell, T. L.; Boyd, C. L.; Dubberley, S. R.; Sealey, A. J.; Cowley, A. R.; Skinner, M. E. G.; Mountford, P. New Titanium Imido Synthons: Syntheses and Supramolecular Structures. *Inorg. Chem.* **2005**, *44*, 2882–2894. (d) Adams, N.; Cowley, A. R.; Dubberley, S. R.; Sealey, A. J.; Skinner, M. E. G.; Mountford, P. Evaluation of the Relative Importance of Ti–Cl...H–N Hydrogen Bonds and Supramolecular Interactions Between Perfluorophenyl Rings in the Crystal Structures of $[\text{Ti}(\text{NR})\text{Cl}_2(\text{NHMe}_2)_2]$ ($\text{R} = \text{iPr}$, C_6H_5 or C_6F_5). *Chem. Commun.* **2001**, 2738–2739.
- (18) (a) Parsons, T. B.; Hazari, N.; Cowley, A. R.; Green, J. C.; Mountford, P. Synthesis, Structures, and DFT Bonding Analysis of New Titanium Hydrazido(2-) Complexes. *Inorg. Chem.* **2005**, *44*, 8442–8458. (b) Clulow, A. J.; Selby, J. D.; Cushion, M. G.; Schwarz, A. D.; Mountford, P. Synthesis, structures and reactivity of Group 4 hydrazido complexes supported by calix[4]arene ligands. *Inorg. Chem.* **2008**, *47*, 12049–12062.
- (19) Fletcher, D. A.; McMeeking, R. F.; Parkin, D. The United Kingdom Chemical Database Service. *J. Chem. Inf. Comput. Sci.* **1996**, *36*, 746–759 (The UK Chemical Database Service: CSD version 745.738 updated May 2017)..
- (20) Lorber, C.; Choukroun, R.; Vendier, L. A General and Facile One-Step Synthesis of Imido–Titanium(IV) Complexes: Application to the Synthesis of Compounds Containing Functionalized or Chiral Imido Ligands and Bimetallic Diimido Architectures. *Eur. J. Inorg. Chem.* **2006**, 2006, 4503–4518.
- (21) Addison, A. W.; Rao, T. N.; Reedijk, J.; van Rijn, J.; Verschoor, G. C. Synthesis, structure, and spectroscopic properties of copper(II) compounds containing nitrogen–sulphur donor ligands; the crystal and molecular structure of aqua[1,7-bis(N-methylbenzimidazol-2'-yl)-2,6-dithiaheptane]copper(II). *J. Chem. Soc., Dalton Trans.* **1984**, 1349–1356.
- (22) Aullón, G.; Bellamy, D.; Brammer, L.; Bruton, E. A.; Orpen, A. G. Metal-bound chlorine often accepts hydrogen bonds. *Chem. Commun.* **1998**, 653–654.
- (23) Komorowski, L.; Meller, A.; Niedenzu, K. Boron nitrogen-compounds. 124. Pyrazole derivatives of 9-borabicyclo[3.3.1]nonane. *Inorg. Chem.* **1990**, *29*, 538–541.
- (24) (a) Owen, C. T.; Bolton, P. D.; Cowley, A. R.; Mountford, P. Cyclopentadienyl Titanium Imido Compounds and Their Ethylene Polymerization Capability: Control of Molecular Weight Distributions by Imido N-Substituents. *Organometallics* **2007**, *26*, 83–92. (b) Carmalt, C. J.; Newport, A. C.; Parkin, I. P.; White, A. J. P.; Williams, D. J. Titanium Imido complexes as precursors to titanium nitride. *J. Chem. Soc., Dalton Trans.* **2002**, 4055–4059.
- (25) Lyne, P. D.; Mingos, D. M. P. Investigation of the *trans* influence in transition metal nitride complexes. *J. Chem. Soc., Dalton Trans.* **1995**, 1635–1643.
- (26) Collier, P. E.; Dunn, S. C.; Mountford, P.; Shishkin, O. V.; Swallow, D. Exchange of Organoimido Groups at a Mononuclear Titanium Centre and a Crystallographic Evaluation of the Relative Structural Influences of the NBU^t , $\text{NC}_6\text{H}_4\text{Me}$ -4 and $\text{NC}_6\text{H}_4\text{NO}_2$ -4 Ligands. *J. Chem. Soc., Dalton Trans.* **1995**, 3743–3745.
- (27) (a) Odom, A. L. New C–N and C–C bond forming reactions catalyzed by titanium complexes. *Dalton Trans.* **2005**, 225–233. (b) Ciszewski, J. T.; Harrison, J. F.; Odom, A. L. Investigation of transition metal-imido bonding in $\text{M}(\text{NBU}^t)_2(\text{dpma})$. *Inorg. Chem.* **2004**, *43*, 3605–3617. (c) Patel, S.; Li, Y.; Odom, A. L. Synthesis, Structure, and LLCT Transitions in Terminal Hydrazido(2-) Bipyridine Complexes of Titanium. *Inorg. Chem.* **2007**, *46*, 6373–6381.
- (28) Guiducci, A. E.; Cowley, A. R.; Skinner, M. E. G.; Mountford, P. Novel double substrate insertion versus isocyanate extrusion in reactions of imidotitanium complexes with CO_2 : critical dependence on imido N-substituents. *J. Chem. Soc., Dalton Trans.* **2001**, 1392–1394.
- (29) Bai, Y.; Noltemeyer, M.; Roesky, H. W. Synthesis and structures of monoalkylamides and monoalkylimides of titanium. *Z. Naturforsch., B: J. Chem. Sci.* **1991**, *46*, 1357–1363.
- (30) (a) Guiducci, A. E.; Boyd, C. L.; Mountford, P. Reactions of cyclopentadienyl-amidinate titanium imido compounds with CS_2 , COS , isocyanates and other unsaturated organic substrates. *Organometallics* **2006**, *25*, 1167–1187. (b) Guiducci, A. E.; Boyd, C. L.; Clot, E.; Mountford, P. Reactions of cyclopentadienyl-amidinate titanium imido compounds with CO_2 : cycloaddition-extrusion vs. cycloaddition-insertion. *Dalton Trans.* **2009**, 5960–5979.
- (31) Coles, M. P.; Hitchcock, P. B. Exploration of the Suitability of Bicyclic Guanidines as Ligands in Catalytic Chemistry Mediated by Titanium. *Organometallics* **2003**, *22*, 5201–5211.
- (32) (a) Li, Y.; Banerjee, S.; Odom, A. L. Synthesis and Structure of (Triphenylsilyl)imido Complexes of Titanium and Zirconium. *Organometallics* **2005**, *24*, 3272–3278. (b) Majumder, S.; Gipson, K. R.; Staples, R. J.; Odom, A. L. Pyrazole Synthesis Using a Titanium-Catalyzed Multicomponent Coupling Reaction and Synthesis of Withasomnine. *Adv. Synth. Catal.* **2009**, *351*, 2013–2023.
- (33) Bartlett, R. A.; Chen, H.; Rasika Dias, H. V.; Olmstead, M. M.; Power, P. P. Synthesis and Spectroscopic and Structural Characterization of the Novel Lithium Borylamide Salts $\text{trans}[\text{Li}(\text{Et}_2\text{O})\text{-NHBMes}_2]_2$, a Dimer, and the Ion Pair $[\text{Li}(\text{Et}_2\text{O})_3][\text{Mes}_2\text{BNBMes}_2]$ with a Linear Allene-like, $[\text{R}_2\text{B}=\text{N}=\text{BR}_2]^-$, Moiety. *J. Am. Chem. Soc.* **1988**, *110*, 446–449.
- (34) Bader, R. F. W. *Atoms in Molecules: A Quantum Theory*; Oxford University Press: Oxford, 1990.
- (35) Swallow, D.; McInnes, J. M.; Mountford, P. Titanium Imido Complexes with Tetraaza Macrocyclic Ligands. *J. Chem. Soc., Dalton Trans.* **1998**, 2253–2259.
- (36) Reed, A. E.; Curtiss, L. A.; Weinhold, F. Natural Bonding Orbital analysis. *Chem. Rev.* **1988**, *88*, 899–926.
- (37) Bent, H. A. An Appraisal of Valence-bond Structures and Hybridization in Compounds of the First-row elements. *Chem. Rev.* **1961**, *61*, 275–311.
- (38) (a) Dunn, S. C.; Mountford, P.; Robson, D. A. Cyclopentadienyl, indenyl and bis(cyclopentadienyl) titanium Imido compounds. *J. Chem. Soc., Dalton Trans.* **1997**, 293–304. (b) Smith, M. R.; Matsunaga, P. T.; Andersen, R. A. Preparation of Monomeric $(\text{Me}_5\text{C}_5)_2\text{VO}$ and $(\text{Me}_5\text{C}_5)_2\text{Ti}(\text{O})(\text{L})$ and their decomposition to $(\text{Me}_5\text{C}_5)_4\text{M}_4(\mu\text{-O})_6$. *J. Am. Chem. Soc.* **1993**, *115*, 7049–7050. (c) Sweeney, Z. K.; Polse, J. L.; Andersen, R. A.; Bergman, R. G.; Kubinec, M. G. Synthesis, structure and reactivity of monomeric titanocene sulfido and disulfido complexes. Reaction of H_2 with a terminal $\text{Ti}=\text{S}$ bond. *J. Am. Chem. Soc.* **1997**, *119*, 4543–4544. (d) Doxsee, K. M.; Farahi, J. B. Synthesis and reactivity of vinylimido complexes of titanocene. *J. Chem. Soc., Chem. Commun.* **1990**, 1452–1454. (e) Howard, W. A.; Parkin, G. Multiple bonds between hafnium and the chalcogens: synthesis and structures of the terminal chalcogenido complexes $(\eta\text{-C}_5\text{Me}_4\text{R})_2\text{Hf}(\text{E})(\text{NC}_5\text{H}_5)$ ($\text{E} = \text{O}, \text{S}, \text{Se}, \text{Te}$). *J. Organomet. Chem.* **1994**, *472*, C1–C4. (f) Zuckerman, N. L.; Bergman, R. G. Structural factors that influence the course of overall $[2 + 2]$ cycloaddition reactions between $\text{Cp}_2\text{Zr}=\text{NR}$ and heterocumulenes. *Organometallics* **2000**, *19*, 4795–4809. (g) Carney, M. J.; Walsh, P. J.; Bergman, R. G. The generation of reactive intermediates $\text{Cp}^*_2\text{Zr}=\text{S}, \text{O}$: trapping reactions with unsaturated organic molecules

- and dative ligands. *J. Am. Chem. Soc.* **1990**, *112*, 6426–6428.
- (h) Walsh, P. J.; Baranger, A. M.; Bergman, R. G. Stoichiometric and catalytic hydroamination of alkynes and allene by zirconium $\text{Cp}_2\text{Zr}(\text{NHR})_2$. *J. Am. Chem. Soc.* **1992**, *114*, 1708–1719.
- (i) Hou, Z.; Breen, T. L.; Stephan, D. W. Formation and reactivity of the early metal phosphides and phosphinidenes $\text{Cp}^*_2\text{Zr}=\text{PR}$, $\text{Cp}^*_2\text{Zr}(\text{PR})_2$ and $\text{Cp}^*_2\text{Zr}(\text{PR})_3$. *Organometallics* **1993**, *12*, 3158–3167.
- (j) Baranger, A. M.; Walsh, P. J.; Bergman, R. G. Variable regiochemistry in the stoichiometric and catalytic hydroamination of alkynes by imidozirconium complexes caused by an unusual dependence of the rate law on alkyne structure and temperature. *J. Am. Chem. Soc.* **1993**, *115*, 2753–2763.
- (k) Howard, W. A.; Waters, M.; Parkin, G. Terminal zirconium oxo complexes: synthesis, structure and reactivity of $(\text{C}_5\text{Me}_5)_2\text{Zr}(\text{O})(\text{NC}_5\text{H}_4\text{R}')$. *J. Am. Chem. Soc.* **1993**, *115*, 4917–4918.
- (l) Howard, W. A.; Parkin, G. Terminal oxo, sulfido, selenido and tellurido complexes of zirconium, $(\eta\text{-C}_5\text{Me}_5)_2\text{Zr}(\text{E})(\text{NC}_5\text{H}_5)$: Comparison of Zr–E single and Zr:E double bond lengths. *J. Am. Chem. Soc.* **1994**, *116*, 606–615.
- (m) Sweeney, Z. K.; Polse, J. L.; Bergman, R. G.; Andersen, R. A. Dihydrogen Activation by Titanium Sulfide Complexes. *Organometallics* **1999**, *18*, 5502–5510.
- (39) Polse, J. L.; Andersen, R. A.; Bergman, R. G. Reactivity of a terminal Ti(IV) imido complex towards alkenes and alkynes: cycloaddition vs C–H activation. *J. Am. Chem. Soc.* **1998**, *120*, 13405–13414.
- (40) Haehnel, M.; Ruhmann, M.; Theilmann, O.; Roy, S.; Beweries, T.; Arndt, P.; Spannenberg, A.; Villinger, A.; Jemmis, E. D.; Schulz, A.; Rosenthal, U. Reactions of Titanocene Bis(trimethylsilyl)acetylene Complexes with Carbodiimides: An Experimental and Theoretical Study of Complexation versus C–N Bond Activation. *J. Am. Chem. Soc.* **2012**, *134*, 15979–15991.
- (41) Hermanek, S. ^{11}B NMR Spectra of Boranes, Main-Group Heteroboranes, and Substituted Derivatives. Factors Influencing Chemical Shifts of Skeletal Atoms. *Chem. Rev.* **1992**, *92*, 325–362.
- (42) Doxsee, K. M.; Garner, L. C.; Juliette, J. J.; Mouser, J. K. M.; Weakley, J. R.; Hope, H. Titanocene Imido Complexes: Generation as Reactive Intermediates, Isolation, and Structural Characterization. *Tetrahedron* **1995**, *51*, 4321–4332.
- (43) (a) Anhaus, J. T.; Kee, T. P.; Schofield, M. H.; Schrock, R. R. Planar “20-electron” osmium imido complexes. A linear imido ligand does not necessarily donate its lone pair of electrons to the metal. *J. Am. Chem. Soc.* **1990**, *112*, 1642–1643. (b) Schofield, M. H.; Kee, T. P.; Anhaus, J. T.; Schrock, R. R.; Johnson, K. H.; Davis, W. M. Osmium imido complexes: synthesis, reactivity, and SCF-X α -SW electronic structure. *Inorg. Chem.* **1991**, *30*, 3595–3604. (c) Benson, M. T.; Bryan, J. C.; Burrell, A. K.; Cundari, T. R. Bonding and structure of heavily π -loaded complexes. *Inorg. Chem.* **1995**, *34*, 2348–2355. (d) Morrison, D. L.; Wigley, D. E. Multiple-imido complexes of molybdenum: synthesis and reactivity of the d^0 $\text{Mo}(=\text{NR})_3$ functional group. *Inorg. Chem.* **1995**, *34*, 2610–2616. (e) Benson, M. T.; Cundari, T. R.; Moody, E. W. Methane activations by tris(imido) complexes: the effect of metal, ligand and d orbital occupation. *J. Organomet. Chem.* **1995**, *504*, 1–3.
- (44) (a) Glueck, D. S.; Green, J. C.; Michelman, R. I.; Wright, I. N. Study of Metal-Ligand Multiple Bonding in Osmium and Iridium Imido Complexes: Evidence for the Cyclopentadienyl-Imido Analogy. *Organometallics* **1992**, *11*, 4221–4225. (b) Williams, D. S.; Schofield, M. H.; Anhaus, J. T.; Schrock, R. R. Synthesis and reactions of tungsten(IV) bis(imido) complexes: relatives of bent metallocenes. *J. Am. Chem. Soc.* **1990**, *112*, 6728–6729.
- (45) Crabtree, R. H.: *The Organometallic Chemistry of the Transition Metals*, 4th ed.; Wiley Blackwell: London, 2005.
- (46) (a) Green, J. C. Bent metallocenes revisited. *Chem. Soc. Rev.* **1998**, *27*, 263–271. (b) Silavwe, N. D.; Bruce, M. R. M.; Philbin, C. E.; Tyler, D. R. Descriptive Photochemistry and Electronic Structure of the Cp_2MoO and $(\text{MeCp})_2\text{MoO}$ Complexes ($\text{Cp} = \eta^5\text{-C}_5\text{H}_5$; $\text{MeCp} = \eta^5\text{-CH}_3\text{C}_5\text{H}_4$). *Inorg. Chem.* **1988**, *27*, 4669–4676. (c) Green, J. C.; Green, M. L. H.; James, J. T.; Konidaris, P. C.; Maunder, G. H.; Mountford, P. Bis(η -cyclopentadienyl)-molybdenum and -tungsten Imido Complexes: X-Ray Structures of $[\text{Mo}(\eta\text{-C}_5\text{H}_5)_2(\text{NBU}^t)]$ and $[\text{Mo}(\eta\text{-C}_5\text{H}_4\text{Me})_2(\text{NBU}^t)\text{Me}]$. *J. Chem. Soc., Chem. Commun.* **1992**, 1361–1365. (d) Jorgensen, K. A. MO explanation of the “unexpected” structure of $(\eta^5\text{-C}_5\text{Me}_5)_2\text{Ta}(=\text{NC}_6\text{H}_5)\text{H}$. *Inorg. Chem.* **1993**, *32*, 1521–1522. (e) Hanna, T. E.; Keresztes, I.; Lobkovsky, E.; Bernskoetter, W. H.; Chirik, P. J. Synthesis of a Base-Free Titanium Imido and a Transient Alkylidene from a Titanocene Dinitrogen Complex. *Organometallics* **2004**, *23*, 3448–3458. (f) Bridgeman, A. J.; Davis, L.; Dixon, S. J.; Green, J. C.; Wright, I. N. Electronic Structure of 20-electron bis(cyclopentadienyl)-metal oxo compounds of group 6: Investigation by photoelectron spectroscopy. *J. Chem. Soc., Dalton Trans.* **1995**, 1023–1027. (g) Hanna, T. E.; Lobkovsky, E.; Chirik, P. J. Dihydrogen and Silane Addition to Base-Free, Monomeric Bis(cyclopentadienyl)titanium Oxides. *Inorg. Chem.* **2007**, *46*, 2359–2361. (h) Luo, L.; Lanza, G.; Fragaia, I. L.; Stern, C. L.; Marks, T. J. Energetics of metal-ligand multiple bonds. A combined solution and thermochemical and ab initio quantum chemical study of $\text{M}=\text{O}$ bonding in group 6 metallocene oxo complexes. *J. Am. Chem. Soc.* **1998**, *120*, 3111–3122.
- (47) Lauher, J. W.; Hoffmann, R. Structure and chemistry of bis(cyclopentadienyl)- ML_n complexes. *J. Am. Chem. Soc.* **1976**, *98*, 1729–1742.
- (48) Marsella, J. A.; Folting, K.; Huffman, J. C.; Caulton, K. G. Transition-Metal-Mediated Hydrogenation of CO to Olefins: Intermediacy of Coordinated Carbenes. *J. Am. Chem. Soc.* **1981**, *103*, 5596–5598.
- (49) (a) Lu, E.; Li, Y.; Chen, Y. A scandium terminal imido complex: synthesis, structure and DFT studies. *Chem. Commun.* **2010**, *46*, 4469–4471. (b) Scott, J.; Basuli, F.; Fout, A. R.; Huffman, J. C.; Mindiola, D. J. Evidence for the existence of a terminal imidoscandium compound: Intermolecular C–H activation and complexation reactions with the transient $\text{Sc} = \text{NAr}$ species. *Angew. Chem., Int. Ed.* **2008**, *47*, 8502–8505. (c) Mountford, P.; Ward, B. D. Recent developments in the non-cyclopentadienyl organometallic and related chemistry of scandium. *Chem. Commun.* **2003**, 1797–1803.